# Biological and chemical sensors based on graphene materials

Liu, Yuxin; Dong, Xiaochen; Chen, Peng

2012

Liu, Y., Dong, X., & Chen, P.(2012). Biological and Chemical Sensors based on Graphene Materials. Chemical Society Reviews, 41, 2283-2307.

https://hdl.handle.net/10356/94489

https://doi.org/10.1039/C1CS15270J

Chemical Society Reviews

Dynamic Article Links ►

Cite this: DOI: 10.1039/c0xx00000x

www.rsc.org/xxxxxx

ARTICLE TYPE

# Biological and Chemical Sensors based on Graphene Materials

**Yuxin Liu[a], Xiaochen Dong[a], Peng Chen[a]***

[a]*Division of Bioengineering, School of Chemical and Biomedical Engineering, Nanyang Technological University, Singapore 637457 (Singapore)*
*Corresponding author: Peng Chen (chenpeng@ntu.edu.sg)*

Owing to their extraordinary electrical, chemical, optical, mechanical and structural properties, graphene and its derivatives have stimulated exploding interests in their sensor applications ever since the first isolation of free-standing graphene sheet in year 2004. This article critically and comprehensively review the emerging graphene-based electrochemical sensors, electronic sensors, optical sensors, and nanopore sensors for biological or chemical detection. We emphasize on the underlying detection (or signal transduction) mechanisms, the unique roles and advantages of the used graphene materials. Properties and preparations of different graphene materials, their functionalizations are also comparatively discussed in view of sensor development. Finally, the perspective and current challenges of graphene sensors are outlined. (312 references)

## 1. Introduction

Graphene is a single-atom-thick planar sheet of $sp^2$-bonded carbon atoms perfectly arranged in a honeycomb lattice. Owing to its extraordinary physiochemical and structural properties,[1-5] this exciting new material has quickly sparked tremendous interests across many disciplines, including nanoelectronics and high-frequency electronics [6-8], energy storage and conversion,[9, 10] field emission display,[11, 12] and transparent conductors.[13] In this article, we survey the emerging applications of graphene for biological and chemical sensing.

In the past decade or so, various zero dimensional (0D) and one dimensional (1D) nanomaterials have been the main impetuses for novel and better sensor developments.[14-17] These include quantum dots,[18, 19] nanoparticles,[20, 21] nanowires[22-25], and notably, carbon nanotubes[26-29] that are one-dimensional cylinders of carbon sheet. Ever since the first isolation of free-standing graphene sheet in 2004 [30], this two-dimensional (2D) carbon crystal has been highly anticipated to provide unique and new opportunities for sensor applications. In fact, despite its short history, graphene has already demonstrated great potentials in various novel sensors which utilize graphene's exceptional electrical properties (*e.g.*, extremely high carrier mobility and capacity), electrochemical properties (*e.g.*, high electron transfer rate), optical properties (*e.g.*, excellent ability to quench fluorescence), structural properties (*e.g.*, one-atom thickness and extremely high surface-to-volume ratio), or its mechanical properties (*e.g.*, outstanding robustness and flexibility).

Although graphene has also been used as physical sensors (*e.g.*, for detection of photon[31], magnetic field[32], mass[33, 34] and strain[35]), here, we place the emphases on biological and chemical sensors. We aim to provide a comprehensive review covering the latest developments, and importantly, offer insights on the underlying detection mechanisms and on the unique advantages of graphene in comparison with other materials. We hope that this article would inspire broader interests across various disciplines and stimulate more exciting developments in this still young yet very promising field of research.

## 2. Properties and preparations of graphene materials

Different synthetic routes produce graphene materials with distinct characteristics. In this section, we briefly discuss these preparation methods and the properties of the resulting graphene materials in a comparative way. This discussion shall provide clues for optimal selection of a graphene material for a particular sensor development and help to understand the advantages and disadvantages of the chosen material.

Single-layer graphene (SLG) sheet was first obtained by mechanical cleavage of graphite (figure 1a).[30] The high quality pristine graphene sheet obtained this way is a fascinating model system for condensed-matter physics and has allowed physicists to reveal the fundamental properties of this amazing material. Pristine SLG is a semi-metal with zero energy bandgap. It exhibits remarkably high carrier mobility at room temperature (20000 $cm^2V^{-1}s^{-1}$) ,[36] high carrier density ($10^{13}$ $cm^{-2}$),[36] room temperature Hall effect,[37] low intrinsic noises as compared with other nanostructured materials,[38-40] and ambipolar field-effect characteristics. These exceptional properties are particularly useful for the development of electronic sensors. However, mechanical exfoliation is of low throughput and not able to produce large-sized graphene sheet (typically, limited to a few micrometers). These drawbacks greatly limit the practical use of mechanically exfoliated graphene.

Graphene film can be grown on transition metal substrates (*e.g.*, nickel, copper, palladium) using chemical vapor deposition (CVD) (figure 1c).[41-43] At low pressure, the CVD growth of graphene on copper foil is a self-limiting process, *i.e.*, it automatically stops after a single graphene layer forms.[44] An advantage of CVD growth is that substitutional doping is feasible

by introducing heteroatoms (nitrogen, boron, etc.) into the carbon lattice. The type and the extent of doping can be manipulated. In addition, CVD growth is able to produce large-sized graphene films which ease the sensor device fabrication and provide large detection area. The properties of CVD grown graphene, however, de*via*te to some extent from that of pristine SLG (*e.g.*, decrease in mobility and shift in Dirac point), due to existence of defects, impurities, and few-layered domains. And the necessity to transfer the as-grown graphene film from the metal substrate to an insulating substrate for device fabrication usually introduces additional impurities and limits the actual attainable size for device fabrication.[45]

Another method to obtain arbitrarily large gaphene film is to decompose silicon carbide (SiC) to graphene at high temperatures.[46] An important advantage of this method is that

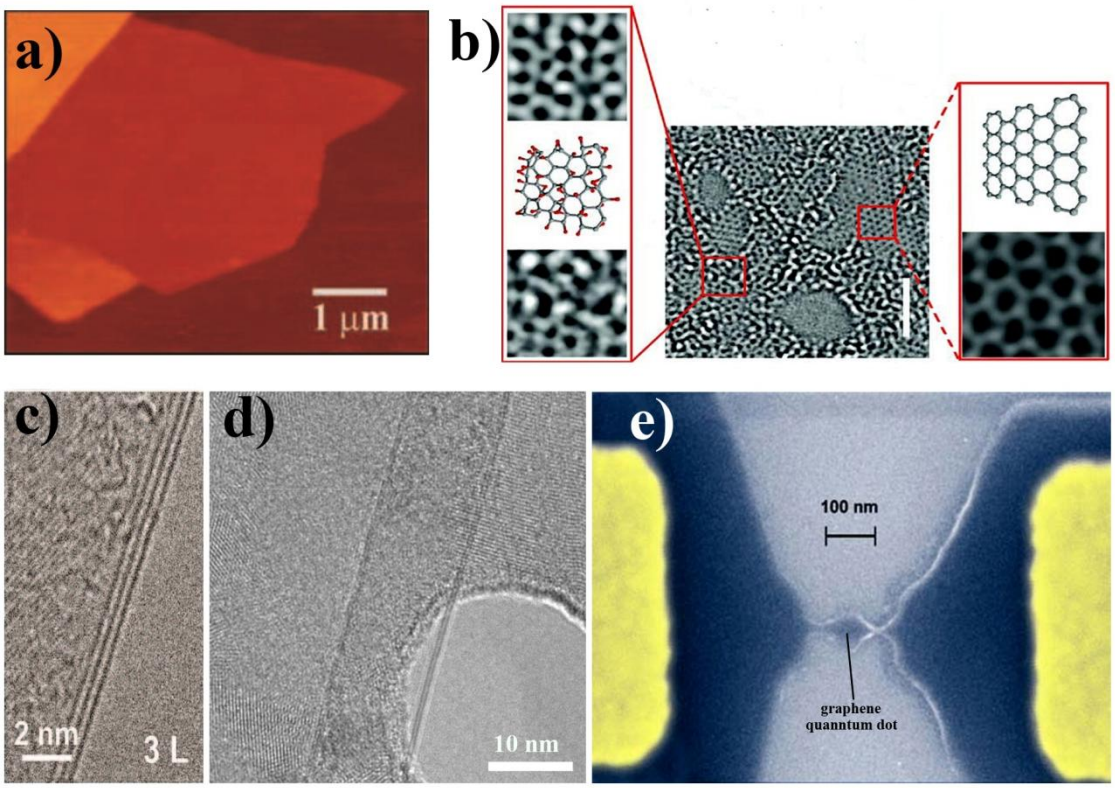


**Figure 1** Different graphene materials. (a) Atomic force microscopy (AFM) image of a single-layer graphene obtained by mechanical cleavage of graphite. Adapted with permission from ref 30. Copyright 2004 SCIENCE (b) Aberration-corrected transmission electron microscopy (TEM) image of a single sheet of suspended graphene oxide. The scale bar is 2 nm. Left expansion shows, from top to bottom, a 1 $nm^2$ enlarged oxidized region of the material, then a proposed atomic structure of this region with carbon atoms in gray and oxygen atoms in red, and finally the average of a simulated TEM image of the proposed structure and a simulated TEM image of another structure where the position of oxidative functionalities has been changed. Right expansion shows a 1 $nm^2$ graphitic portion from the exit plane wave reconstruction of a focal series of GO and the atomic structure of this region. Adapted with permission from ref 59. Copyright 2010 WILEY-VCH Verlag GmbH & Co. KGaA, Weinheim (c) High magnification TEM images showing the edges of film regions consisting of 3 layers of CVD grown graphene. The cross-sectional view is enabled by the folding of the film edge. Adapted with permission from ref 43. Copyright 2009 American Chemical Society. (d) TEM image of a graphene nanoribbon suspended over porous silicon grids, showing nearly atomically smooth edges. Adapted with permission from ref 70 Copyright 2009 American Chemical Society. (e) The scanning electron micrograph (in false color) illustrates a graphene quantum dot device. Adapted with permission from ref 83 Copyright 2008 SCIENCE

transfer process is not required because SiC itself is a good insulator. Therefore, large integrated circuits with hundreds of transistors can be carved on a single large-size epitaxial graphene on SiC using standard microelectronics technologies.[47] Conceivably, sensor array with integrated amplification and processing circuits may be similarly made on an as-grown graphene film. An interesting phenomenon has been reported that the interaction between graphene and SiC substrate opens the graphene bandgap to ~0.26 eV.[48] This is desired for field-effect transistors (FETs) and also for sensors whose detection relies on the induced field-effect. However, it is difficult to precisely control the properties of graphene epitaxially grown on SiC, which depend on the face of SiC used for graphene formation and the edge-termination (silicon or carbon). In addition, decomposition of SiC is not self-limiting. As a result, the resulting graphene film is heterogeneous in thickness (thus properties).

Chemical reduction of exfoliated graphene oxides (GO) was historically the first method for graphene synthesis, reported by Boehm and co-workers in 1962.[49] The interest of this method is greatly reignited after demonstration of the remarkable properties of mechanically exfoliated graphene, because it provides a facile route for low-cost mass-production of graphene, more accurately, reduced graphene oxide (RGO) or chemically derived graphene (CDG).[50] In addition to chemical reduction (most commonly, by hydrazine), RGO can also be obtained by thermal,[51]

photothermal,[52] or electrochemical reduction.[53] Nevertheless, the properties of RGO are substantially different from that of pristine graphene, due to the defects in the $sp^2$ hybridized carbon lattice and a variety of oxygenated groups irreversibly caused by the oxidative process for chemical exfoliation of graphene oxides from graphite.[54] Although relativistic charge transport and some other condensed-matter effects observed in the pristine material are absent in RGO, its facile and scalable preparation, unique and tunable properties make it attractive for sensor applications. And the chemical groups on RGO provide convenient handles for surface modifications, for example, for covalent anchorage of the recognition elements against specific sensing targets. Since GO can dissolve in water and various solvents, solution-based processes (*e.g.*, inkjet printing, microfluidic patterning, spray-coating) together with in-situ reduction can be employed to readily fabricate RGO thin-film devices on arbitrary substrates, for example, on a flexible substrate that can conformably attach onto a curved sensing object.[55] Moreover, RGO is more electrochemically active as compared to pristine graphene owing to the abundant reactive sites at edges and in defective basal plane,[56] promising its use in electrochemical sensors.

Graphene oxides (GO), commonly obtained by placing graphite in a mixture of strong acid(s) and oxidizing agent(s)[57, 58], not only is the precursor of RGO but also may serve as a sensing element itself. It is a heterogeneous, non-conductive, and atomically thin sheet with nano-sized $sp^2$ carbon clusters isolated by oxygenated $sp^3$ carbon domains (figure 1b).[50, 59, 60] In contrast to pristine graphene, GO is photoluminescent over a broad range of wavelengths due to quantum-confinement induced bandgap opening in the heterogeneously sized $sp^2$ clusters. On the other hand, GO is also a highly efficient fluorescence quencher. These optical properties suggest its potentials in optical detection.[61] The size, shape, composite, and relative fraction of $sp^3$-hybridized domains of GO can be chemically, thermally, or electrochemically engineered to manipulate GO's optoelectronic properties, for example, transforming it from an insulator to a semiconductor or to a graphene-like semi-metal.[60] RGO obtained from intense reduction of GO exhibits similar ambipolar characteristics with a low on-off ratio as that of pristine graphene, albeit with a much lower carrier mobility. RGO resulted from mild reduction can acquire a high on-off ratio because its transport is dominated by the voltage-dependent carrier tunneling or hopping between $sp^2$ clusters.[62] Such voltage dependent transport may be utilized for electronic sensing. Taken together, GO and RGO provide tunable, versatile and powerful platforms for various sensing applications. To preserve the crystalline carbon structure (hence the ballistic transport properties), graphene can be non-covalently exfoliated in liquid phase, using molecules that can effectively intercalate between the stacked graphene layers in graphite.[63-66] But it should be kept in mind that those intercalating agents usually remain firm association with graphene sheet and unavoidably alter its electronic structure.

The properties of graphene can be drastically modified or fine-tuned by atomistic or chemical doping.[67, 68] Its properties also depend on its dimension, layer structure, and edge configuration. When one lateral dimension of graphene shrinks to nanoscale becoming graphene nanoribbons (GNRs), it may transform to a semiconductor with a large bandgap due to quantum confinement of the electron wave function[69]. GNR can be obtained by longitudinally unzipping carbon nanotubes using gas-phase oxidation followed by sonication[70] (Figure 1d), chemical attacking by $H_2SO_4$ and $KMnO_4$ [71], lithium intercalation,[72] catalytic cutting by metal nanoparticles,[73] plasma etching on carbon nanotube partially embedded in polymeric matrix,[74] cutting by hydrogen,[75] electrochemical unzipping,[76] electrical unwrapping,[77] or laser cutting.[78] Alternatively, GNRs can be produced by templated growth on SiC,[79] surface-assisted bottom-up synthesis,[80] or top-down lithographic fabrication.[81] Two-dimensionally shrinking a graphene sheet to nanoscale results in a graphene quantum dot (GQD) which may operate as a single-electron transistor.[82] GQD can be carved from graphene using nanolithography[83, 84] (figure 1e) or be produced by hydrothermal cleavage of GO.[85] Both GNR and GQD are highly sensitive to the field-effect and to chemical disruption at edges, therefore providing opportunities for ultrasensitive detection. In addition, their small dimensions permit spatially resolved or highly localized detection. Layer number is another important factor to influence the properties of graphene. It has been shown that, in contrast to zero bandgap single-layered graphene, bilayer graphene exhibits a continuously and widely tunable electronic bandgap up to 0.25 eV.[86]

As discussed above, the properties of graphene materials can be controlled by the synthetic conditions, dimensions, layer numbers, and doping. Such tunable and diverse properties of graphene materials provide vast possibilities for various sensing purposes. The selection of specific graphene material should be made according to the specific sensing target and the sensing mechanism to be utilized, with a balanced consideration on performance (*e.g.*, detection limit and dynamic range), reproducibility, cost, and manufacturability. In the article, for clarity, we sometimes generally refer all forms of graphene related materials as graphene in general discussions. But when sensor examples are discussed, the specific type of graphene material used will be unambiguously indicated (*e.g.*, mechanically exfoliated graphene, CVD grown graphene, RGO, GO, and so on). For more comprehensive information on graphene properties and preparations, the readers may consult the previous reviews and references therein.[67, 87-93]

## 3. Graphene Functionalization

To endow graphene with sensing capabilities, it is often necessary to functionalize it with recognition elements that bring the detection targets onto graphene surface through specific interactions and sometimes also assist in signal transduction. Graphene may also be functionalized in order to enhance its sensitivity, specificity, loading capacity, biocompatibility, etc. Various strategies have been devised to functionalize graphene's 1D cousin, carbon nanotubes (CNTs).[94] These strategies could be adopted straightforwardly for graphene. As compared to the narrow CNTs (1-2 nm in diameter), 2D graphene is more amenable to effective, reproducible, and homogeneous functionalization. Here we briefly discuss the approaches to modify graphene and divide them into two general categories: covalent and noncovalent. For detailed chemistry, the readers may refer to several previous articles on this topic. [94-98]

### 3.1 Covalent methods

Chemical moieties, commonly, carboxylic (-COOH) and hydroxyl (-OH) groups, can be covalently created on graphene surface using strong acids and/or oxidants. Exfoliated by oxidation process, GO (also its reduced form -RGO) is populated with these oxygen-containing chemical groups. Fluorine, which is one of the strongest oxidants, can readily react with carbon materials including graphene. Different kinds of chemical moieties (*e.g.*, amino, hydroxyl, or alkyl groups) may then be introduced onto graphene by substituting the fluorine atoms due to the weak (highly reactive) C-F bonds in fluorinated graphene. In addition, microwave-assisted sulfonation has been used to create sulfonate ($-SO_3$) groups[99] while plasma (ammonia or nitrogen plasma) treatment has been used to create amino ($-NH_2$) groups on graphene.[100]

The chemical moieties created on graphene surface can serve as chemical handles to graft functional molecules (*e.g.*, proteins, carbohydrates, polymers) through covalent bonding. For example, carboxylic groups can react with proteins, carbohydrates or other polymers *via* amide or ester linkages. Graphene may also be grafted with functional molecules containing silane tail through salinization with hydroxyl groups on graphene surface by forming Si-O-C bond.[101] Functional molecules can be directly bonded on graphene surface using free-radical addition, Billups reaction, cycloaddition, thermal or photochemical activated C=C addition etc.[94, 102, 103] Covalent functionalization of linker molecules (*e.g.*, a branched polymer with multiple reactive ends) could be used to provide an amplification mechanism for further functionalization of sensing probes and/or to provide a spacing between graphene and sensing probes (or sensing environment). [104]

### 3.2 Noncovalent methods

Although covalent strategies can effectively, stably and specifically install functionalities, they unavoidably alter the native electronic structure and physical properties of graphene by converting $sp^2$ carbons to $sp^3$ ones, *e.g.*, causing severe decrease in carrier mobility. In view of this problem, noncovalent modifications have been employed in order to preserve the intrinsic properties of the original graphene materials.

Various molecules can physically adsorb onto graphene materials without the need of any coupling reagents. Graphene can be viewed as a giant (the largest) aromatic molecule. It can firmly interact with any molecules with aromatic ring(s) on the surface. Graphene materials, for example, GO that is highly negatively charged, are able to electrostatically adsorb oppositely charged molecules. In addition, hydrophobic or Van der Waals interaction may assist the physical adsorption. However, physical adsorption is non-specific. To deal with this issue, passivation molecules (commonly, bovine serum albumin and Tween-20) are often applied to block the unfunctionalized area (sites) in order to avoid non-specific adhesion of unwanted molecules. Similar passivation could also be used after covalent functionalizations to quench the un-reacted sites and block non-active area.[105]

Functional molecules can be immobilized onto graphene through linker molecules, for instance, 1-pyrenebutanoic acid succinimidyl ester whose pyrene group at one end noncovalently binds to graphene surface through strong π-π interaction while the succinimidyl ester group at the other end is reactive to amines on biomolecules.[106] Other bifunctional molecules with aromatic tail and a reactive end (*e.g.* perylene tetracarboxylic acid, thionine and many porphyrin derivatives) can also be employed as linker molecules.[98]

Graphene materials, particularly, GO and RGO, can be non-covalently decorated with metal nanparticles (*e.g.*, Au, Ag, Pt) through in situ reduction,[107, 108] electrospray[109] or electrochemical deposition[110]. These nanoparticles may serve as the catalysts to mediate signal transduction in graphene based sensors, or as the docking points to anchor sensing probes with high capacity. For instance, thiolated biomolecules (*e.g.*, thiol-ssDNA) can be anchored onto gold nanoparticles *via* formation of thio-gold bond.

## 4. Electrochemical sensors

Ever since its discovery, graphene has quickly become a material under spotlight for development of new electrochemical sensors because of its unique electrochemical and structural properties.[111] Since graphene has a large electrochemical potential window (approximately 2.5 V in 0.1 mM phosphate buffer saline solution),[112] detection of molecules that have high oxidation or reduction potential (*e.g.*, nucleic acids) become feasible. In addition, edges and defects on graphene provide high electron transfer rate,[113] suggesting that RGO sheets or small flakes of pristine graphene are superior for electrochemical detection. It has been demonstrated that the electron transfer rate of $Fe^{3+/2+}$ on RGO is more than an order of magnitude higher than that on glassy carbon electrode (GCE) due to the unique electronic structure of RGO, especially the high density of the electronic states over a wide energy range.[114, 115] Electron transfer can be enhanced also because small graphene flakes are able to provide direct electrical wiring between the electrode and the active centers of the redox enzymes.[116] Interestingly, RGO has intrinsic catalytic activity towards some small enzymatic products such as $H_2O_2$ and NADH, making it attractive for enzyme-based sensors. Owing to its extremely high surface-to-volume ratio (theoretically, 2600 $m^2/g$),[117] graphene based electrodes provide a large effective reaction area and high capacity for enzyme loading. High surface-to-volume ratio also makes it ideal for functional composite, in which, a small percentage of graphene is able to provide percolating pathways for charge conduction.

Most graphene based electrochemical sensors use RGO because 1) its abundant defects and chemical groups facilitate charge transfer and thus ensure high electrochemical activity; 2) the populated chemical moieties on RGO surface offer the convenience and flexibility for various functionalizations to enhance the sensor performance; 3) the chemical and electrical properties of RGO are highly tunable; and 4) as compared to non-conductive GO, RGO can efficiently transport charges.

### 4.1 Detecting hydrogen peroxide

Hydrogen peroxide ($H_2O_2$) is an enzymetic product of many biological processes. Therefore, detection of $H_2O_2$ is of great importance. Xu *et al.* fabricated a $H_2O_2$ sensor using a RGO-chitosan composite film entrapped with hemoglobin (Hb) molecules (Figure 2a).[118] It exhibits a lower limit of detection (LOD) (0.51 μM) and a wider linear range (6.5 – 230 μM) as

compared with the conventional $H_2O_2$ detection methods. This is because RGO-chitosan matrix can be abundantly loaded with Hb molecules and provide a biocompatible microenvironment to retain the enzyme in its native structure. Furthermore, RGO facilitates the electron transfer between the matrix and the electroactive center of hemoglobin and the percolating 3D network of RGOs provide multiplexed paths to rapidly conduct

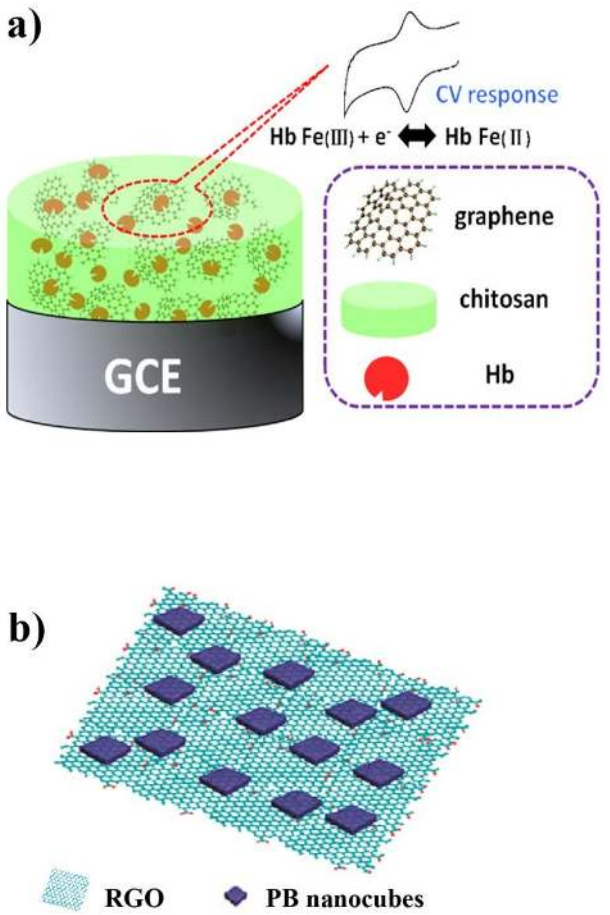


**Figure 2**. Graphene-material based electrochemical sensor for detection of $H_2O_2$. (a) Schematic of the construction of Hb-graphene–chitosan/GCE. Hb = hemoglobin; GCE = glassy carbon electrode; graphene here is actually RGO. Adapted with permission from ref 118. Copyright 2010 Elsevier B.V. (b) Illustration of a RGO sheet decorated with Prussian blue (PB) nanocubes. Adapted with permission from ref 129. Copyright 2010 American Chemical Society.

away the charges. In another $H_2O_2$ sensor, horseradish peroxidase (HRP) was used instead to hydrolyze $H_2O_2$; and small graphene sheets non-covalently exfoliated by the aromatic molecules (tetrasodium 1,3,6,8-pyrenetetrasulfonic acid) were used to anchor the enzymes with large capacity and to efficiently mediate the charge transfer.[119] This sensor gives a detection limit of 0.106 μM and a linear range from 0.63 μM to 16.8 μM. A novel hierarchical nanostructures formed by layer-by-layer assembly of HRP and sodium dodecyl benzene sulphonate (SDBS) functionalized RGO has been reported by Zeng *et al.* for $H_2O_2$ detection.[120] An impressively low detection limit (0.1 μM) was achieved due to the high enzyme loading and the fact that enzymes intercalated in RGOs retain high catalytic efficiency towards $H_2O_2$ with low diffusion barrier. Single-stranded DNAs (ssDNA) which can interact with graphene or RGO through π-π stacking have been utilized to assist material dispersion, to electrostatically attract reactants, or to enhance the loading of enzymes.[121, 122]

Electrochemical detection of $H_2O_2$ can also be catalyzed by metal nanoparticles. Using one-step microwave-assisted thermal reduction, Wang and co-workers have fabricated a platinum nanoparticle/RGO hybrid for $H_2O_2$ detection.[123] The detection limit of this sensor (80 nM) is several orders lower than other carbon-based electrodes, such as, the CNTs/chitosan modified electrode (10.3 μM),[124] the highly ordered mesoporous carbon modified electrode (1.61 μM),[125] CNTs/silica/Au/Pt hybrid nanomaterial (0.5 μM).[126] And a broad range of linear response is achieved (1 μM-500 μM). The high performance of this sensor can be attributed to the facts that platinum nanoparticles can be uniformly deposited on RGO nanosheets with high density, and rapid charge transfer is ensured by the intimate interaction between metal nanoparticles and RGO and their highly conductive nature. The same group also demonstrated a similar sensor based on gold nanoparticle / RGO hybrid.[127] Zhou *et al.* incorporated RGO with both nanoparticles (gold) and enzymes (microperoxidase-11), in which gold nanoparticles not only act as the catalyst but also act synergistically with RGO sheets to facilitate charge transfer.[128] The highest sensitivity (45 nM) in all $H_2O_2$ sensors is realized by decorating RGO thin-film with in-situ grown Prussian blue which is a superior electrocatalyst (artificial peroxidase) for $H_2O_2$ reduction (Figure 2 b).[129]

### 4.2 Detecting glucose

Mediated by specific enzymes, the excellent sensing ability of graphene-based electrochemical sensors towards $H_2O_2$ can be utilized to detect other molecules, oxidation of which produces $H_2O_2$. For example, glucose can be detected by using glucose oxidase (GOD) as the mediator or recognition element.

Conducting porous matrix, which gives large effective detection surface and high enzyme loading capacity, can be made by mixing RGO with supporting polymers. Kang and co-workers reported a GOD–RGO–chitosan modified electrode that exhibited a wider linear range (from 0.08 mM to 12 mM), a lower LOD (0.02 mM), and a higher sensitivity (37.93 μA $mM^{-1}cm^{-2}$), as compared with the sensors using other nanostrucrtured materials.[130] The electron-transfer-rate constant (2.83±0.18 $s^{-1}$) of this senor is higher than that of multi-walled carbon nanotubes (MWCNTs) based sensors.[131, 132] Without using chitosan that may hinder electron transfer, a simple electrode with GOD adsorbed on RGO thin film was fabricated.[133] It offers a LOD of 0.01 mM and sensitivity of 110.0 μA $mM^{-1}$ $cm^{-2}$. Alwarappan *et al.* constructed a porous matrix with GOD, RGO, and polypyrrole (ppy). The ppy provides excellent conductivity, support to the matrix, and biocompatibility. A ultra-low LOD (3 μM) was reached.[134] A layer-by-layer (LbL) assembly of alternating RGO films and poly(ethyleneimine) (PEI) films with controllable film thickness, morphology, and composition has also been presented.[135] Both glucose oxidase and glucoamylase were loaded into such LbL film to enable simultaneous detection of glucose and maltose, demonstrating the possibility of integrating RGO and multi-enzyme systems in a single multilayer film.

Various strategies have been developed to modify RGO. For

instance, ionic liquids have been used to hybridize with RGO.[136, 137] Ionic liquids assist to disperse RGO for thin-film fabrication, and can serve as excellent binders between electrolyte and electrode because of their ability to promote electron transfer and ion exchange, their electrochemical stability and biocompatibility. Au nanoparticles have been used to decorate RGO by in-situ reduction or physical adsorption to improve LOD, detection range, and stability.[112, 138] Similarly, platinum nanoparticles have been electrochemically deposited on RGO and an outstanding LOD of 0.6 μM has been achieved for glucose detection.[110] RGO can also be modified by doping. Nitrogen-doped (N-doped) RGO film that possesses large amount of positive charges can improve the electrochemical detection by enhancing adsorption of $O_2$, $H_2O_2$ and other intermediates.[139] Wang *et al.* developed a novel sensor based on N-doped RGO/Chitosan/GOD/GCE hybrid.[140] It has a detection limit as low as 10 μM. The reduction potential of the electrode was shifted by 400 mV towards positive potential as compared with bare GCE, indicating its fast electron transfer kinetics.

### 4.3 Detecting nucleic acids

Graphene materials have also been employed for sensitive and selective electrochemical detection of nucleobases, nucleotides, single stranded DNAs (ssDNA), and double stranded DNAs (dsDNA). Such electrochemical DNA sensor may provide a simple alternative approach for DNA analysis and sequencing.

The four distinct nucleobases (A: adenine, T: thymine, C: cytosine, G: guanine) can be electrochemically differentiated because they have different oxidation potentials. Huang *et al.* used RGO with abundant –COOH groups to electrochemically detect guanine and adenine with a LOD of 50 nM and 25 nM, respectively.[141] The high sensitivity can be ascribed to the excellent electrochemical properties of RGO, the electrostatic attraction between the negatively charged –COOH groups and the positively charged nucleobases, and the strong π-π stacking interaction between the nucleobases and honeycomb carbon lattice. A $Fe_3O_4$ nanoparticle doped RGO-chitosan electrode has been used to detect guanosine.[142] It was suggested that $Fe_3O_4$ nanoparticles help to reduce the electron transfer resistance.

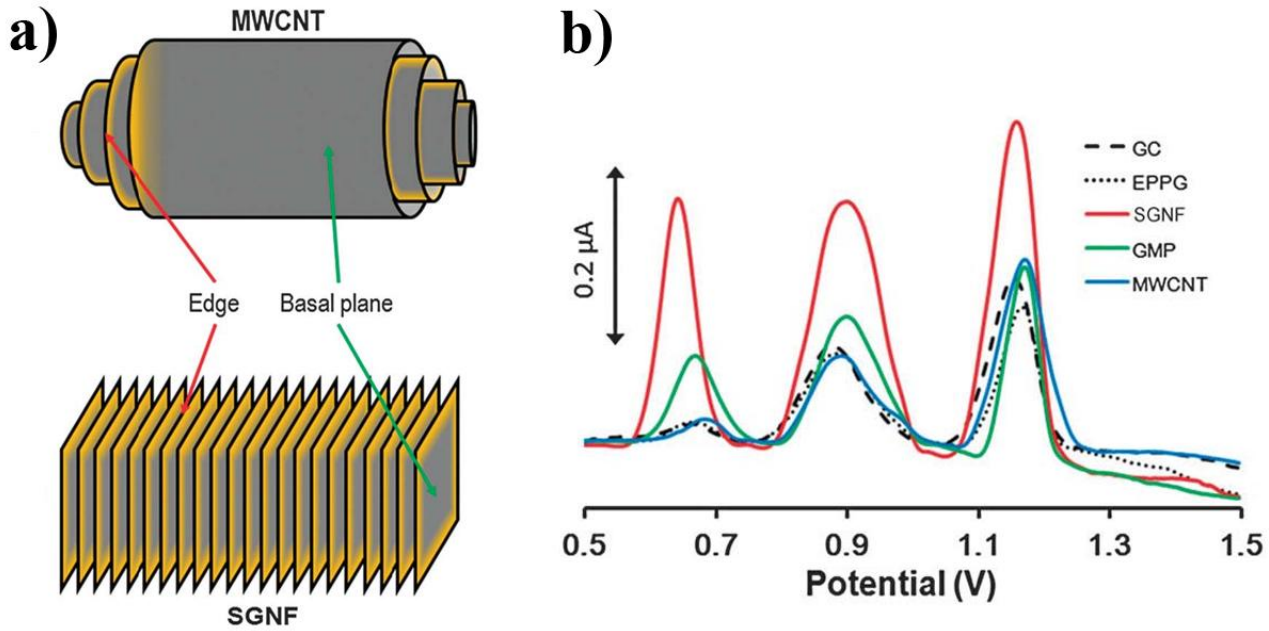


**Figure 3**. Graphene-based electrochemical DNA sensor. (a) Schematics of graphene sheet orientation in multiwalled carbon nanotubes (upper) and stacked graphene nanofibers (lower). The highly electroactive edge portion of the sheets is represented in yellow. (b) Differential pulse voltammetry (DPV) for ssDNA of the human influenza A(H1N1) obtained from SGNF (stacked graphene nanofiber, red), GMP (graphite microparticle, green), MWCNT (multi-walled carbon nanotube, blue), GC (glassy carbon, black dashed), and EPPG (edge plane pyrolytic graphite, black dotted) electrodes. Adapted with permission from ref 144. Copyright 2010 the Owner Societies

Du and co-workers fabricated a RGO electrode decorated with AuNPs by potentiostatic electrodeposition to detect ssDNA.[143] The incorporation of AuNPs was proven to be essential to separate the oxidation signal of T from that of A. And they demonstrated that the electrochemically reduced RGO showed enhanced electrochemical and electrocatalytic activity as compared to chemically reduced RGO. This DNA sensor is able to detect single-base alteration (mutation) without any labeling or probe DNA. Stacked graphene nanofibers (SGNFs) was used by Ambrosi *et al.* to distinguish the four nucleobases with a sensitivity two to four folds higher than carbon nanotube-based electrodes (Figure 3).[144] The high sensitivity is due to numerous open edges of individual graphene nanosheets which are much more electrochemically active comparing to the basal carbon plane. This sensor was employed to examine the base composition of human influenza A(H1N1) DNA strand. In the work of Lim *et al.*, graphene epitaxially grown on SiC was used to detect dsDNA.[145] It was shown that dsDNA can be differentiated from ssDNA, because dsDNA exhibits lower oxidation peaks for A and C and increased oxidation potential for C. Electrochemical detection of dsDNA is not possible with the conventional electrodes (*e.g.*, gold electrode and GCE) due to

their limited electrochemical potential window. The authors also demonstrated that electrochemical anodization to introduce oxygenated groups onto graphene largely improved the electrode performance.

A GO modified electrode was used for detection of DNA hybridization.[146] In this work, probe ssDNA molecules that are lack of guanine base were covalently immobilized onto GO film, and hybridization was detected by the guanine oxidation signal from the target ssDNA molecules (a hepatitis B virus specific sequence). In an interesting demonstration by Zhao *et al.*, RGO quantum dots (~10 nm) were used to modify the pyrolytic graphite electrode for detection of DNA hybridization.[147] When the target ssDNA hybridizes with the pre-immobilized probe ssDNA, the electron transfer from the electrochemically active species $[Fe(CN)_6]^{3-/4-}$ was increased because the blocking effect by the probe ssDNA was alleviated. A LOD of 100 nM was reached. This study suggests the potentials of RGO quantum dots in electrochemical sensing. The good performance of RGO quantum dots may be attributed to their abundant edge sites (electrochemical active sites) and quantum confinement effects. Based on similar sensing scheme, Wang *et al.* showed a RGO based sensor to detect hybridization of methicillin-resistant *staphylococcus aureus* DNA with a LOD of 100 fM.[148] However, the authors proposed an opposite mechanism. They argued that hybridized DNAs remained on the RGO surface and caused an increase of electron transfer resistance (hence a decrease in electrochemical signal). The discrepancy between Zhao's work and Wang's work may be because of the size difference between RGO quantum dots and RGO sheets. Larger RGO sheets likely can bind more strongly with hybridized DNAs.

Hypoxanthine is a purine derivate. A hypoxanthine sensor was constructed using an electrode consisting of RGO, conducting polypyrrole graft copolymer - poly(styrenesulfonic acid-g-pyrrole), and enzyme xanthine oxide.[149] The detection mechanism of such sensor involved two-steps of oxidation: oxidation of hypoxanthine under the catalysis of xanthine oxide, and subsequent oxidation of uric acid and $H_2O_2$ produced from the previous reaction. RGO and the conducting polymer interact with π-π stacking and form a nanocomposite with high conductivity and excellent electrocatalytic environment. As a result, a LOD of 10 nM was obtained. As hypoxanthine accumulates continuously from adenine nucleotide degradation after fish death, this sensor was employed to assess fish freshness.

### 4.4 Detecting protein markers

Graphene based electrochemical sensors have also been developed to detect various protein biomarkers. Su *et al.* fabricated a label-free immunosensor to specifically detect cancer marker alpha fetoprotein (AFP) using layer-by-layer construction with electropolymerized thionine (TH) film, GO-chitosan composite, AuNPs, and conjugates of horseradish peroxidase (HRP) and anti-AFP antibody.[150] Binding of AFP molecules to the antibodies partially blocks the active center of HRP and consequently decreases the catalytic reduction of $H_2O_2$ by HRP (thus decrease in electrochemical signal). The electroactive TH acts synergistically with HRP to mediate the electron transfer from $H_2O_2$ to the electrode. The achieved LOD (0.7 ng/ml) is much better than the conventional enzyme-linked immunosorbent assays (ELISA). This sensor was challenged with clinical human serum samples and the negative/positive samples were correctly identified in accordance with the results from a commercial clinical device. A simpler AFP sensor was made by incorporating TH with RGO film through π-π interaction followed by covalent crosslinking of AFP antibodies with TH.[151] Binding of AFP molecules blocks the electron-transfer and mass-transfer, leading to a decrease of electrochemical signal originated from the redox reactions of TH. In comparison with other sensors, such as, carbon nanotube or nanoparticle derived AFP sensors, a much lower LOD (5.77 $pgmL^{-1}$) was achieved, due to the high electron transfer rate between the intimately interacted RGO and TH, and high loading of TH molecules and AFP-antibodies because of the large surface area provided by RGO film. The sensor was successfully used to determine AFP in serum samples.

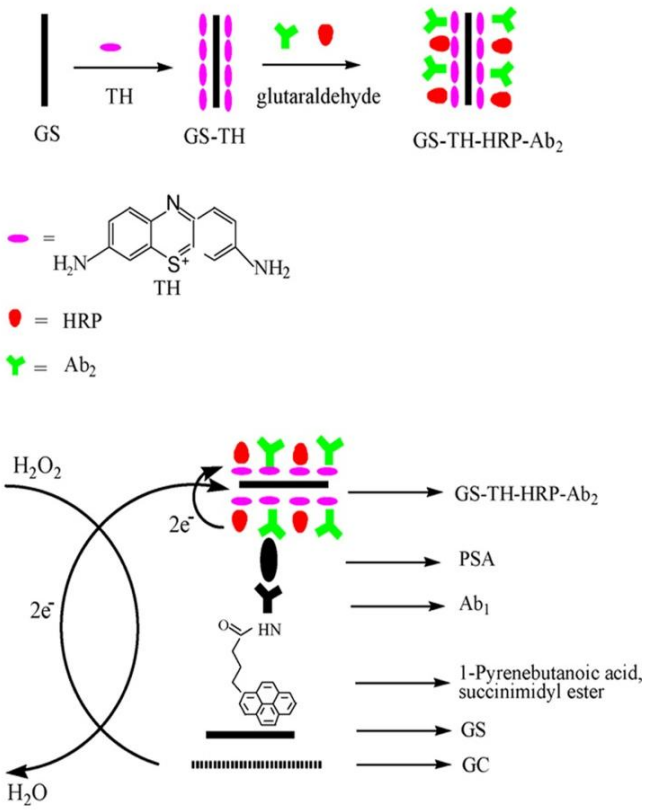


**Figure 4**. Schematic illustration of an electrochemical immunosensor for detection of prostate specific antigen (PSA). GS = reduced graphene oxide sheet; TH = thionine; HRP = horseradish peroxidase; Ab2 = secondary anti-PSA antibody; Ab1 = primary anti-PSA antibody; GC = glassy carbon electrode. Adapted with permission from ref 153. Copyright 2010 Elsevier B.V.

Du *et al.* used a different strategy to detect AFP.[152] In their work, AFP molecules bound to the primary-antibody-functionalized RGO electrode complex again with carbon nanospheres (CNS) tagged with the secondary antibodies and HRP molecules, leading to an increased electrochemical signal from redox reaction of $H_2O_2$. The use of RGO and CNS gave a 7-fold increase in the detection sensitivity, because of the superior electrochemical and electrical properties of RGO and the ability of CNS to carry multiple HRP molecules. A 20 pg/ml LOD was

demonstrated. A similar sensor to detect prostate-specific antigen (PSA) (marker for prostate cancer) based on sandwich immunoreactions on top of RGO modified electrode has been reported (Figure 4).[153] In comparison with Du's work, CNS was replaced by small RGO flake, because RGO flake can carry more secondary antibodies and more HRP molecules due to its extremely large surface-to-volume ratio. Here, dual functionalities of RGO were utilized, *i.e.*, firstly as the electrode material and secondly as the enzyme carrier. An impressive detection limit of 1 pg/mL was demonstrated, superior to other PSA sensors including a sensor using carbon nanotube-HRP conjugates.[154] A sandwich-like immunodetection of carcinoembryonic antigen (CEA) which is a marker for colorectal cancer was developed by Zhong *et al.*[117] In their work, a nanocomposite of gold nanoparticles (AuNPs), RGO and chitosan was used to carry multi-copies of HRP-conjugated CEA-specific secondary antibody onto a glassy carbon electrode modified with Prussian blue and AuNP. 10 pg/mL CEA can be detected. In another demonstration, a RGO modified electrode for sandwich-like immunodetection of immunoglobulin G (IgG) in human serum was developed.[155]

### 4.5 Detecting other biomolecules

Dopamine (DA) is an important neurotransmitter, deficiency of which underlies Parkinson's diseases. DA detection is challenged by its low physiological concentration (0.01 μM - 1 μM) and interference from much more abundant ascorbic acid (AA) and uric acid (UA). A chitosan-RGO composite electrode for DA detection was demonstrated by Wang *et al.*[156] A linear detection range (5 – 200 μM) was achieved in the presence of a large excess of AA or UA (500 μM). In addition, they showed that chitosan-RGO electrode outperformed the electrode made of chitosan and multi-walled carbon nanotubes. Hou *et al.* demonstrated an electrochemical sensor to selectively detect dopamine with a LOD of 0.01 μM based on a composite electrode made of Nafion and *N*-(trimethoxysilylpropyl) ethylenediamine triacetic acid (EDTA) modified RGO.[101] The high performance arises from several reasons: 1) dopamine can interact with RGO *via* π-π interaction; 2) EDTA groups, combined with ionic sulfuric groups of Nafion, can concentrate DA from the solution; 3) EDTA groups linked to the RGO surface promote electron transfer as evidenced by the narrower potential separation between the anodic and cathodic peaks ($\Delta E_p$); 4) the oxygen containing functional groups on RGO block the diffusion of AA and thus eliminate its interference. In another work, detection of DA at 5 nM was realized in presence of excess AA using a β-cyclodextrin/RGO nanocomposite electrode.[157] β-cyclodextrin functionalization assists dispersion of RGO sheets, and greatly improves the electrochemical performance. As compared with the bare RGO electrodes, the β-cyclodextrin/RGO electrodes exhibited a two-orders-of-magnitude-lower LOD, attributable, at least in part, to the faster electron transfer rate ($\Delta E_p$ was reduced from 115 mV to 73 mV).

AA and UA sensors have also been developed using graphene materials. For example, Keeley *et al.* demonstrated an AA sensor using graphene nano-sheets exfoliated in liquid by dimethylformamide (DMF).[65] A UA sensor was constructed by self-assembling gold nanoparticles (AuNP) onto pyrenebutyrate functionalized RGO (PFG) sheets.[158] A LOD of 0.2 μM was obtained. Shang *et al.* utilized a novel microwave plasma enhanced CVD method to obtain multilayer graphene nanoflake films (MGNFs) vertically grown on silicon substrate.[159] DA, AA, and UA can be unambiguously distinguished by three well-defined peaks appeared in the cyclic voltammogram (CV). Furthermore, near-ideal electron transfer kinetics was evidenced by the narrow $\Delta E_p$ (61.5 mV at the scan rate of 10 mV/s) which is close to the ideal value of 59 mV. Such fast electron transfer process is due to the abundant edge planes and defects on the nanoflakes, unique electronic structure of graphene, and the good electrical contact between MGNFs and silicon substrate.

Cholesterol is an essential constitute of cell membrane.[160] However, undesired accumulation of cholesterol and its esters causes critical health problems, such as, heart diseases, cerebral thrombosis, and artherosclerosis. A sensitive amperometric sensor based on functionalized RGO sheets has been developed for detection of cholesterol and its esters with a LOD of 0.2 μM.[161] Cholesterol esterases and cholesterol oxidases were loaded onto the electrode to catalyze the hydrolysis of cholesterol and its esters, and consequently, generate $H_2O_2$. Platinum nanoparticles decorated on RGO sheets, in turn, catalyze the electrochemical oxidization of $H_2O_2$. Nafion coating was used at the same time to block other irrelevant analytes (*e.g.*, ascorbate and urate).

### 4.6 Cellular detection

Detecting rare pathological cells is of obvious clinical significance. Feng and co-workers fabricated a sensitive and selective RGO-based electrochemical biosensor to detect cancer cells with overexpressed nucleolin on plasma membrane (*e.g.* breast cancer cells and human cervical carcinoma cells), at a LOD of thousand cells /mL.[162] To avoid RGO aggregation and introduce more -COOH groups, 3,4,9,10-perylene tetracarboxylic acid (PTCA) was used to composite with RGO. And the nanocomposite was covalently functionalized with $NH_2$-modified nucleolin-specific aptamers (oligonucleotides serving as highly selective antibodies) as the recognition element. The binding of cancer cells increases the electron transfer resistance by blocking the access of the redox probe ($[Fe(CN)_6]^{3-/4-}$).

Electrochemical detection in amperometry mode provides high temporal resolution (millisecond). Therefore, it is suitable to detect dynamic cellular activities in real-time. A RGO based senor for detection of the real-time kinetics of oxygen release from human erythrocytes in response to $NaNO_2$ stimulation has been shown.[163] Two kinds of excellent mediators for $O_2$ reduction, namely, laccase (Lac) and 2,2-azino-bis(3-ethylbenzothiazoline-6-sulfonic acid) (ABTS), were functionalized onto RGO sheets to form Lac-ABTS-RGO hybrid electrode. $O_2$ level as low at 10 μM can be detected by this hybrid electrode.

Cellular release of reactive oxygen species (such as $H_2O_2$) is an early indicator for cytotoxic events and cellular disorders. A RGO based electrochemical sensor has been coupled with live human breast cancer cells (MCF-7) to detect triggered cellular release of $H_2O_2$ in real-time and with a LOD of 0.1 μM.[164] To construct the electrode, RGO sheets were first electrophoretically deposited on the indium tin oxide (ITO) glass. This was followed by electrodeposition of Prussian blue (artificial $H_2O_2$ catalyst) and adsorption of extracellular matrix proteins (laminin) to

promote cell adhesion. Ten layers of RGO-PB-laminin were formed on the ITO substrate using layer-by-layer deposition. In situ, real-time, sensitive, and quantitative detection of extracellular $H_2O_2$ release from live cells was demonstrated. Specifically, it was determined that, upon stimulation of phorbol-12-myristate-13-acetate (PMA, 5 μg/mL), $10^{11}$ $H_2O_2$ molecules were released from a single MCF-7 cell over 25s.

### 4.7 Detecting other chemicals

Graphene based electrochemical sensors have also been employed to detect environmental contaminants (paraoxn,[165] nitromethane,[166] heavy metal ions,[167-169] hydroquinone and catechol,[170] methyl jasmonate,[171] hydrazine[172]) pharmaceutical compounds (paracetamol,[173] 4-aminophenol,[174] aloe-emodin,[175] Rutin,[176] etc.), industrial compounds (ethanol[177]), and explosives (TNT[178]).

## 5. Electronic Sensors

Nanoelectronic sensing based on one-dimensional (1D) semiconducting nanomaterials (*e.g.*, carbon nanotubes, silicon nanowires) is an emerging sensing modality that offers high sensitivity, high temporal resolution, simple label-free detection scheme, and suitability for development of lab-on-a-chip devices.[14, 22, 28] Silicon nanowire (SiNW) is perhaps the mostly explored 1D material for nanoelectronic sensing with great successes.[23, 179-181] However, a major limitation of SiNW sensors is that their detection relies essentially on the induced field-effect. Therefore, they are only suitable to the detection of charged analytes or electrogenic events. Two-dimensional graphene has been added as a new building block for nanoelectronic sensors, taking advantages of its extraordinary electrical properties. It provides vast new possibilities.

Graphene exhibits remarkably high carrier mobility, high carrier density, and low intrinsic noises. These characteristics promise high signal-to-noise ratio in detection. And the conductance of graphene is highly sensitive to the local electrical and chemical perturbations because every atom of a graphene film is exposed to the environment. In addition, the Fermi level of zero-bandgap graphene can be modulated by the gate voltage, therefore, the charge carriers can be either holes or electrons depending on the gate voltage. Such ambipolar property allows readily setting of the desired working point. When detection is based on field-effect, large bandgap is desired. The bandgap of graphene can be opened by reducing its dimension(s) to nanoscale[182, 183] or by introducing atomistic or chemical dopants.[63, 184, 185] Moreover, as compared to 1D nanostructured sensing elements, the 2D structure of graphene can provide a larger detection area, and homogeneous surface for uniform and effective functionalization. And it is more suitable to intimately interface with flat cell membranes. It has been shown that graphene is able to support cell adhesion and growth, indicating its biocompatibility.[186, 187] In addition, the outstanding optical transparency of graphene allows simultaneous electrical measurement and optical observation. The ballistic transport property of graphene, however, deteriorates to some extent in RGO due to its defective nature. On the other hand, as discussed earlier, RGO offers rich chemistry for functionalization; can be obtained through facile, scalable and low-cost syntheses; enables solution-based fabrication; and possesses tunable electrical properties.

### 5.1 Detection mechanisms

Graphene electronic sensors are usually referred as field-effect transistors (FETs) because, similar to the conventional FETs, graphene conductance can be sensitively modulated by minute gating signals. This, however, is somewhat misleading because it implies that the detection is achieved only through the field-effect introduced by the sensing targets. But actually, graphene-based electronic detection can be realized through other mechanisms as well, such as, doping effects, charge carrier scattering, change of local dielectric environment. Therefore, graphene nanoelectronic sensors provide a versatile platform for a wide spectrum of sensing purposes.

In solution, a thin ionic double-layer or Debye layer (<1 nm in thickness at physiological ionic strength) forms on top of graphene, which creates a large double-layer capacitance ($C_{dl}$). $C_{dl}$ is much larger than the capacitance of the dielectric gate layer (typically >100 nm in thickness) in back-gated graphene FETs. Therefore, the transconductance (the ratio of drain-source current change over gate voltage change) of liquid-gated graphene FETs is >100 times larger than that of back-gated FETs.[188, 189] Although the overall field-effect of graphene is not prominent, significant current response of graphene to minute field-effect induced by charged molecules or cellular electrical activities is guaranteed by the enhanced transconductance in solution as well as the high conductivity and low noise of graphene.

Graphene electronic sensors can also utilize the doping effects (direct charge transfer between the absorbed analytes and the graphene) because the zerogap electronic structure of graphene is amenable to charge transfer, even with molecules that have a small chemical-potential mismatch. Many molecules, particularly, those possessing aromatic rings, can intimately interact with graphene. Such strong interactions strengthen the doping effect and consequently allow sensitive electronic detection. It has been suggested that open-shell adsorbates can directly transfer charges to or from graphene, causing strong doping effects.[190] Close-shell adsorbates are not able to directly transfer charge with graphene. But they may produce 'indirect doping' by altering the charge distribution within graphene or influencing the existed doping from the supporting substrate or 'impurities' on graphene. Another form of 'indirect doping' is electrochemical doping while charge-donating redox reactions occur at the graphene surface.[191] When Gibbs free energy of the reaction plus the energy required for electron transfer is negative, redox reaction and charge transfer occur spontaneously on graphene surface.

Alterations of local dielectric environment may underlie the graphene device response too. For example, binding of biomolecules could alter the local dielectric constant or local ionic strength, which, in turn, modulates $C_{dl}$ and thus carrier density in graphene.[189, 192] Such dielectric changes could also affect the screening of impurity on graphene surface or long-range electrostatic interaction between the graphene and the substrate, resulting in measurable change in the transport current.[189]

Scattering effect is another sensing mechanism that can be exploited. Adsorbates may cause scattering of electrons or holes,

and consequently decrease carrier mobility thus conductance of graphene.[38] Oppositely, adsorbates may alleviate the scattering effect caused by the supporting substrate, leading to an increase in graphene conductance.[193, 194] Furthermore, detection may arise from pH change,[105] expansion or deformation of graphene lattice,[195-197] or the modulation of the Schottky energy barrier between the graphene film and the metal electrodes or between the individual flakes in a graphene network.[198] In some cases, detection is determined by a dominant mechanism while, in other cases, it results from the combination of several mechanisms. Therefore, scrutiny is required to interpret the sensor response.

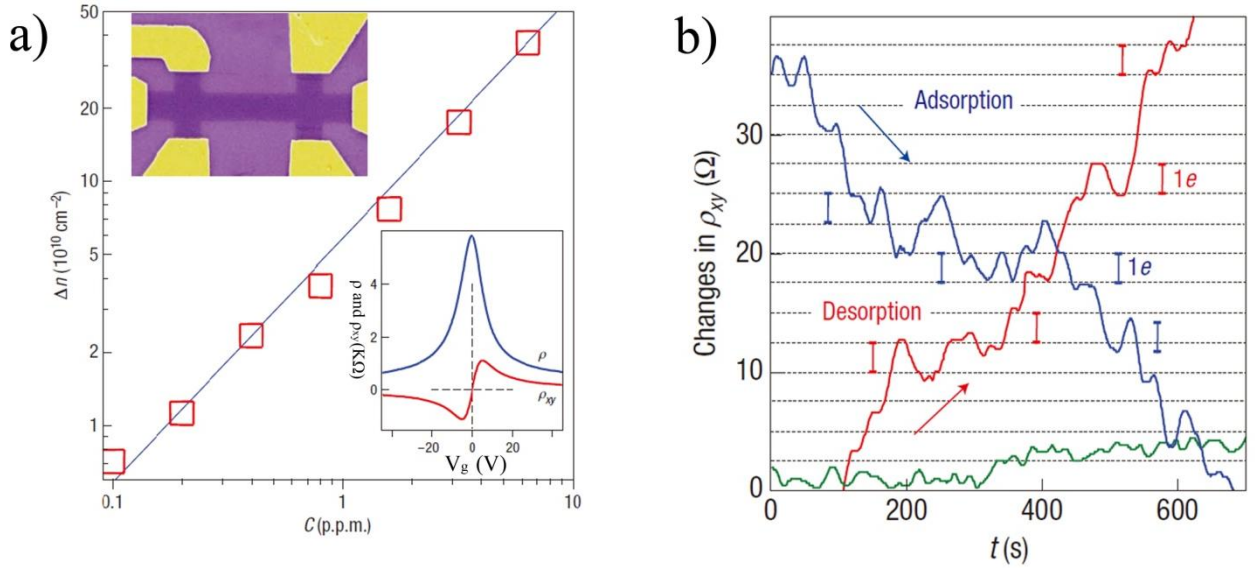


**Figure 5**. Electronic detection of individual gas molecules adsorbed on mechanical exfoliated single-layer graphene. (a) Concentration (Δn) of chemically induced charge carriers in graphene exposed to different concentrations (C) of $NO_2$. Upper inset: scanning electron micrograph of this device. Lower inset: characterization of the graphene device by using the electric-field effect. (b) Examples of changes in Hall resistivity of a three-layer device observed near the neutrality point during adsorption of strongly diluted $NO_2$ (blue curve) and its desorption in vacuum at 50℃ (red curve). The green curve is a reference—the same device thoroughly annealed and then exposed to pure He. To measure Hall resistivity, $\rho_{xy}$, B =10 T was applied perpendicular to graphene's surface. The curves are for a three-layer device in B =10 T. The grid lines correspond to changes in $\rho_{xy}$ caused by adding one electron charge, e($\delta R \approx 2.5\Omega$), as calibrated in independent measurements by varying Vg. For the blue curve, the device was exposed to 1 p.p.m. of $NO_2$ leaking at a rate of $\approx 10^{-3}$ mbar1 $s^{-1}$. Adapted with permission from ref 38. Copyright 2007 Nature Publish Group

### 5.2 Detecting gases

The very first graphene sensor is actually an electronic one for gas detection, demonstrated by Novoselov and co-workers (Figure 5).[38] It used mechanically-exfoliated few-layer pristine graphene as the sensing element and was applied to detect $NO_2$ gas (an open shell molecule). By measuring the change of source-drain resistance, 1 ppb $NO_2$ can be detected. Strikingly, by monitoring the change of the Hall resistance, adsorption or desorption of single $NO_2$ molecule can be clearly resolved as a step-like signal originated from transfer of single electron. This ultimate sensitivity achieved at room temperature is due to that graphene conductance is extremely responsive to the minute environmental perturbation, and also because of the extremely low intrinsic noise of nearly-defect-free graphene. Few-layer (3-5 layers) graphene were most electrically quiet because of their low contact resistance with the metal electrodes. The authors also demonstrated that graphene ~1 μm in size provided the optimal signal-to-noise ratio. Smaller devices exhibited higher 1/f noise because defects at the edges become more prominent, while larger devices gave smaller relative change of resistance. This remarkable study has stimulated tremendous enthusiasm to develop graphene electronic sensors.

Various gas sensors based on graphene materials have been demonstrated thereafter.[198-202] For example, a $NO_2$ sensor was fabricated by placing a RGO micro-sheet between two Au electrodes.[198] Electron transfer from RGO to adsorbed $NO_2$ molecules caused hole enrichment in the p-type RGO sheet and consequently increased its conductance. To accelerate the sensor recovery, low-temperature heating and UV illumination were used to de-adsorb the gas molecules. Commonly, graphene devices are made on $Si/SiO_2$ substrates. Nomani *et al.* demonstrated that 6H-SiC substrates are better than the conventional Si/SiO2 substrates because the interaction between C-face of SiC and graphene leads to less scattering events (thus higher conductivity and lower noise).[203] As a result, graphene sensors fabricated on 6H-SiC substrate can detect $NO_2$ at a lower concentration (10 ppb)[203] as compared to the graphene sensors made on $Si/SiO_2$ substrates.[204] Jeong *et al.* developed a flexible $NO_2$ gas sensor by growing vertically aligned carbon nanotube array on RGO thin-film network using plasma enhanced CVD to form a nanocarbon hybrid on polyimide substrate.[199] A stable performance can be maintained even under extreme bending owing to the excellent mechanical flexibility of RGO film. Another flexible $NO_2$ sensor was demonstrated by Dua *et al.* which provides a ultralow LOD (~400 ppt).[201] RGO thin-film network was inkjet-printed on poly-(ethylene terephthalate) (PET) plastic film. The authors attributed the high sensitivity to two reasons: 1) the mild reduction agent used (ascorbic acid) introduces less defects as compared with the common agent (hydrazine); 2) the RGO film is highly uniform due to the controllable inkjet-printing process on PET substrate.

Dinitrotoluene (DNT), a highly volatile chemical, is often

detected as a reporter of explosive trinitrotoluene (TNT). A DNT sensor was realized using spin-coated RGO thin-film.[202] Similar to $NO_2$, DNT is a *p*-type dopant with strong electron-withdrawing ability. A detection limit of 28 ppb was obtained, which is much lower than the vapour pressure (173 ppb) of DNT at 298K. A similar RGO sensor constructed by Robinson *et al.* showed a markedly improved LOD (0.1 ppb) for DNT detection.[205] The authors also showed that such RGO sensors are superior to single-walled carbon nanotube (SWCNT) sensors largely due to the much reduced low-frequency (1/f) noise.

Although close-shelled gas molecules are weak dopants, graphene sensors targeting on these gases have also been devised. For instance, a $H_2$ sensor using RGO thin-film was reported by Shafiei *et al.*[206] SiC was employed as the substrate partly because of the high breakdown voltage of the insulating SiC. A platinum (Pt) layer was deposited on top of the RGO film, severing as the catalyst to breakdown $H_2$ molecules. The dissociated hydrogen atoms diffuse into the interface between RGO and Pt and lower the energy barrier between the two materials, thereby promoting the electron transfer from RGO to Pt. As the result, conductance of RGO film is increased due to the increased hole density. It has been suggested that RGO obtained by mild thermal reduction (at 300℃; with final oxygen content of 11.39% on RGO) gives the best sensitivity to $H_2$ due to the optimal trade-off between the conductivity and the density of defect sites for molecular adsorption and catalysis.[207] Johnson *et al.* used palladium (Pd)-coated multi-layer graphene nanoribbon (GNR) networks for $H_2$ detection.[208] High sensitivity (~55% percentage change of resistance to 40 ppm $H_2$ at room temperature) and good repeatability were achieved.

Massera *et al.* demonstrated a RGO based humidity sensor whose conductance increase is proportional to the $H_2O$ increments in the gas carrier.[209] However, such change is not sustainable due to quick de-adsorption of water molecules. This problem is solved by another group using thin-film matrix of RGO and polyvinylpyrrolidone nanosphere which is able to stably trap water molecules inside.[210] The increase of RGO conductance is because the adsorbed water molecules shift the substrate's impurity bands and hence their hybridization with the bands of RGO.

A RGO sensor was developed for detection of a poison gas $H_2S$, with the detection limit of 2 ppm at room temperature.[211] The sensor was fabricated by growing zinc oxide nanorods (ZnO NRs) on RGO. The detection is resulted through two step reactions. Firstly, ambient $O_2$ molecules adsorbed on ZnO NRs are converted into oxygen ionic species, causing a strong p-doping effect on RGO. Such p-doping is then alleviated by $H_2S$ molecules which react with those oxygen ionic species, leading to a conductance increase of the n-type operated RGO.

Lu *et al.* fabricated a RGO sensor to detect $NH_3$ in ambient condition.[212] The authors demonstrated that RGO operated in n-type mode by applying a sufficiently positive gate voltage ($V_g$) gave better performance (*i.e.*, faster response and faster recovery) than biased at p-type mode. The difference could be attributed to the ambipolar transport of RGO and $V_g$-induced effects, such as the change in the graphene work function and the Coulomb interaction between $NH_3$ and graphene. In an interesting work by Yu *et al.*, an electronic $NH_3$ sensor was developed using vertically oriented graphene sheets obtained from plasma-enhanced chemical vapor deposition (PECVD).[213] The authors suggested that such carbon nanowall structure provides large surface area for sensitive detection.

Graphene based electronic sensors have been used to detect other vapours as well, including trimethylamine,[214] HCN,[205] $I_2$,[38] methane,[215] ethanol.[216] It has been suggested that ssDNA decorated on graphene surface can significantly improve the sensing performance by concentrating water and the target vapour molecules.[217]

### 5.3 Chemical detection

A pH sensor using few-layered graphene sheets grown on SiC is the first graphene sensor for detection in solution.[218] By monitoring shift in Dirac (neutral) point, this sensor provides a ultra-Nernstian pH sensitivity (98mV/pH vs. 59.2mV/pH). The authors proposed that the detection mechanism involves pH-dependent surface potential modulation (field-effect) by ion adsorption and the attached amphoteric $OH^-$ groups. Also as suggested by the authors, such high sensitivity is attributable to the high carrier mobility of epitaxial graphene which is an order of magnitude higher than that of hydrogen-terminated diamond or silicon. More recently, Ohno *et al.* investigated pH sensing ability of mechanically exfoliated graphene and found that the detection limit of pH was 0.025, which is more than 26-folds lower than carbon nanotube based electronic pH sensors.[219]

Zhang *et al.* demonstrated a heavy metal sensor using mechanically exfoliated graphene with a detection limit of 10 ppm (~5 μM) for $Hg^{2+}$.[220] Graphene was modified with self-assembled 1-octadecanethiol whose thiol groups have high binding affinity with heavy metal ions. Recently, Chen and co-workers demonstrated a metal ion sensor based on centimeter-long and micrometer-wide RGO thin-film made by microfluidic patterning.[221] By functionalizing $Ca^{2+}$-binding proteins (calmodulin) onto RGO, $Ca^{2+}$ at a concentration of 1 μM can be detected. The detection depends on field-effect induced by the positively charged $Ca^{2+}$ ion. By functionalizing heavy-metal-ion-binding proteins (metallothionein type II protein – MT-II) onto RGO, trace amount (as low as 1 nM) of heavy metal ions (*e.g.*, $Hg^{2+}$, $Cd^{2+}$) can be distinctly detected. The authors proposed that the detection is through the altered field-effect from negatively charged MT-II as it undertakes conformational change upon binding with heavy metal ions. This sensor worked properly with lake water samples which are a complex soup consisting of various ions, microorganisms, and impurities, demonstrating its practical use for environmental monitoring.

Myers *et al.* used octadecylamine (ODA) functionalized RGO nanocomposites as the sensing elements to electrically detect benzene, toluene, ethylbenzene, xylenes and cyclohexane with LOD of ppm.[192] The author proposed that the adsorption of target molecules increases the electron tunnelling barrier between RGO sheets, leading to a decreased conductance.

### 5.4 Biomolecular detection

Graphene electronic biosensors have been developed to detect the building blocks of living beings, such as, saccharides,[106] proteins,[109, 222-224] and DNAs.[99, 225] Chen and co-workers fabricated a CVD-grown graphene sensor to electrically detect glucose and glutamate, with a LOD of ~0.1 mM and ~5 μM

respectively (Figure 6a).[106] The detection is mediated by the functionalized enzymes, specifically, glucose oxidase (GOD) and glutamate dehydrogenase (GluD). The catalytic reactions mediated by both enzymes produce $H_2O_2$, which, being a strong electron withdrawing molecule (p-dopant), can increase the conductance of graphene film operated in p-type regime. The authors also showed that the graphene sensors outperformed thin-film network devices made of single-walled carbon nanotubes.

Most proteins bear charges or dipoles in physiological conditions. This provides possibilities for electronic detection through field-effect or scattering effect. And many proteins possess aromatic-ring-containing amino acids on the surface.

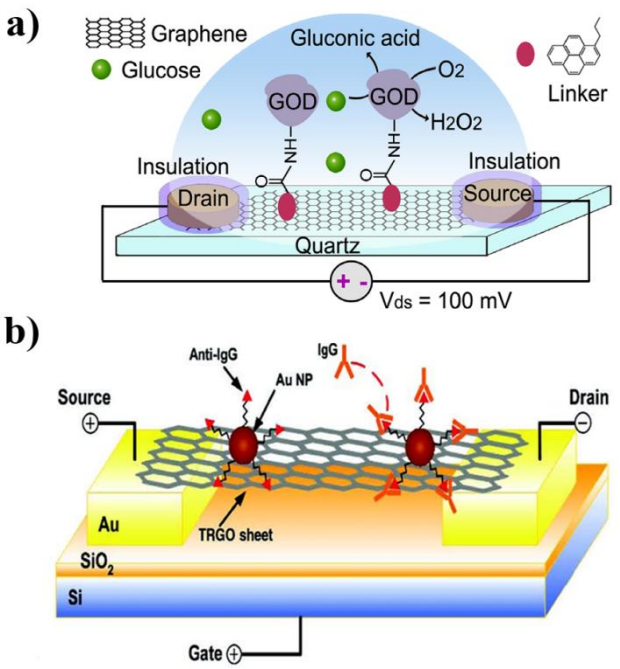


**Figure 6**. Electronic graphene sensors for biomolecular detection. (a) Schematic illustration of glucose oxidase (GOD) functionalized CVD-graphene device for detection of glucose. Adapted with permission from ref 106. Copyright 2010 the Royal Society of Chemistry. (b) Schematic of a FET device based on a suspended thermally-reduced graphene oxide (TRGO) for detection of immunoglobulin G (IgG). Anti-IgG molecules are anchored to the TRGO sheet through gold nanoparticles (Au NPs). Adapted with permission from ref 109. Copyright 2010 WILEY-VCH Verlag GmbH & Co. KGaA, Weinheim

Therefore, they can firmly bind to graphene *via* π-π interaction and therefore may be detected through doping effect. However, due to the complex structure of proteins, the sensor response may be resulted from a single dominant effect (*e.g.*, doping) or be simultaneously influenced by multiple effects depending on the charges, amino acid composition, and orientation of the interacting proteins. So, interpretation on the detection results requires caution. Ohno *et al.* used pristine graphene device to detect bovine serum albumin (BSA) with a LOD as low as 0.3 nM.[222] Non-specific adsorption of BSA molecules caused conductance increase of graphene biased at p-type region, due to field-effect induced by the negatively charged BSA molecules. This sensor, however, is lack of specificity in detection.

In an electronic immunoglobulin E (IgE) sensor, to assure specificity, IgE-specific aptamers were functionalized onto the surface of mechanically exfoliated graphene monolayer *via* a linker molecule (1-pyrenebutanoic acid succinimidyl ester).[226] When the positively charged targets (IgE) were introduced, the conductance of p-typed graphene decreased dramatically due to the field effect. Mao *et al.* developed a RGO thin-film based sensor to detect immunoglobulin G (IgG) with a ultralow detection limit of ~13 pM (Figure 6b).[109] To realize specific detection, AuNP and anti-IgG antibody conjugates were assembled onto RGO sheets by electrospray and electrostatic force directed assembly. In addition, a blocking buffer (a cocktail solution containing tween 20, fish gelatin and BSA) was used to passivate unfunctionalized sites on RGO sheets, so that, non-specific binding of irrelevant molecules was minimized. Similarly, Yang *et al.* reported an immunosensor for detection of prostate specific antigen (PSA) using RGO sheets exfoliated from graphite by thermal expansion method. 1-pyrenebutanoic acid, succinimidyl ester (PBSE) was used as the linker molecule for antibody immobilization and BSA was used to block non-specific binding.[224] A wide linear detection range (0.1 ng/ml – 100 ng/ml), which covers the physiological concentration (1 ng/ml – 10 ng/ml) in human serum, was obtained. In addition, the sensor is re-usable after the treatment with glycine-HCl solution to break the antibody–antigen linkage. The authors proposed that conductance decrease after addition of PSA is due to blocking of current transport between percolating RGO sheets by the intercalating non-conductive PSA molecules.

Recently, an all-RGO device (*i.e.*, conducting channel and source/drain electrodes were all made of RGO thin-film network) fabricated on transparent and flexible substrate was demonstrated by He *et al.* and used as protein sensors.[55] After the RGO channel being biotinylated and subsequently passivated, this device was used to specifically detect avidin with a LOD of ~80 nM based on the p-doping effect from the binding avidin molecules. It is worth mentioning that this sensor is transparent and bendable. The electrical characteristics of the device did not alter even after 5000 bending cycles owing to the excellent flexibility of the RGO film. In an interesting work reported by Myung *et al.*, a chain of RGO-encapsulated $SiO_2$ nanoparticles (NPs) was used as the conducting (sensing) channel.[227] RGO sheets can self-assemble onto 3-aminopropyltriethoxysilane (APTES) modified $SiO_2$ NP (100 nm in diameter). Such 3D nanostructure provides a large surface area for functionalization of recognition elements and thus for detection. By functionalization with specific antibodies, breast cancer biomarkers, human epidermal growth factor receptor 2 (HER2) and epidermal growth factor receptor (EGFR) could be selectively detected with low LOD (100 pM for HER2 and 10 nM for EGFR). Binding of positively charged HER2 or EGFR molecules on RGO surface induces positive gating effect which, in turn, reduces the hole density in the p-type RGO (and hence its electrical conductance).

Graphene electronic sensors have also been employed for detection of DNA molecules. Mohanty *et al.* demonstrated an electronic DNA sensor using a microsized graphene oxide (GO) sheet.[100] Although being called as 'GO' by the authors, the chemically derived graphene used in this work is conductive, *i.e.*, electrically similar to RGO. They functionalized the 'GO' sheets with probe ssDNA *via* simple physical adsorption taking advantage of the firm π-π interaction between DNA bases and

'GO'.[100] Conductance increase of 'GO' was used to indicate the hybridization of the target bacterial ssDNA, as a result of doping effect. It is noted that the electrical measurements were made in dry condition; therefore, DNA molecules are not charged and thus lack of ability to impose field-effect. The authors determined that hybridization of a pair of target and probe ssDNA produces one sixth quantum of hole doping (p-doping). Another DNA sensor was made alternatively with CVD-grown graphene by Dong *et al.*[225] It was able to detect hybridization of target ssDNA in solution with single-base-mismatch specificity and a LOD of 10 fM. The authors suggested that detection (decrease of graphene conductance) is based on DNA induced n-doping on graphene, instead of field-effect and impurity screening mechanism. This is different to the p-doping mechanism in dry condition as proposed by Mohanty *et al.*[100] In addition, Dong and co-workers showed that decoration of gold nanoparticles (AuNPs) can increase the detection range. This is because one AuNP can covalently associate with multiple thiolated probe ssDNA molecules, whereby increases the loading efficiency and capacity. Similar to the results obtained by Dong *et al.*, another team of researchers also observed conductance decrease of their RGO sensor upon DNA hybridization.[228] In that work, a secondary RGO sensor was used as the internal reference to cancel out the common interference, such as, pH change and nonspecific biological adhesion. Choi *et al.* presented a DNA sensor using sulfonated reduced graphene oxide (srGO) through microwave-assisted sulfonation.[99] The $-SO_3$ group on srGO surface provides strong binding sites for immobilization of probe ssDNA. In addition, the srGO sheets can be readily dispersed in water without using dispersion agent and therefore can be readily deposited on a substrate as a uniform ultrathin layer for device fabrication. Consistently, DNA hybridization also caused decrease of srGO conductance.

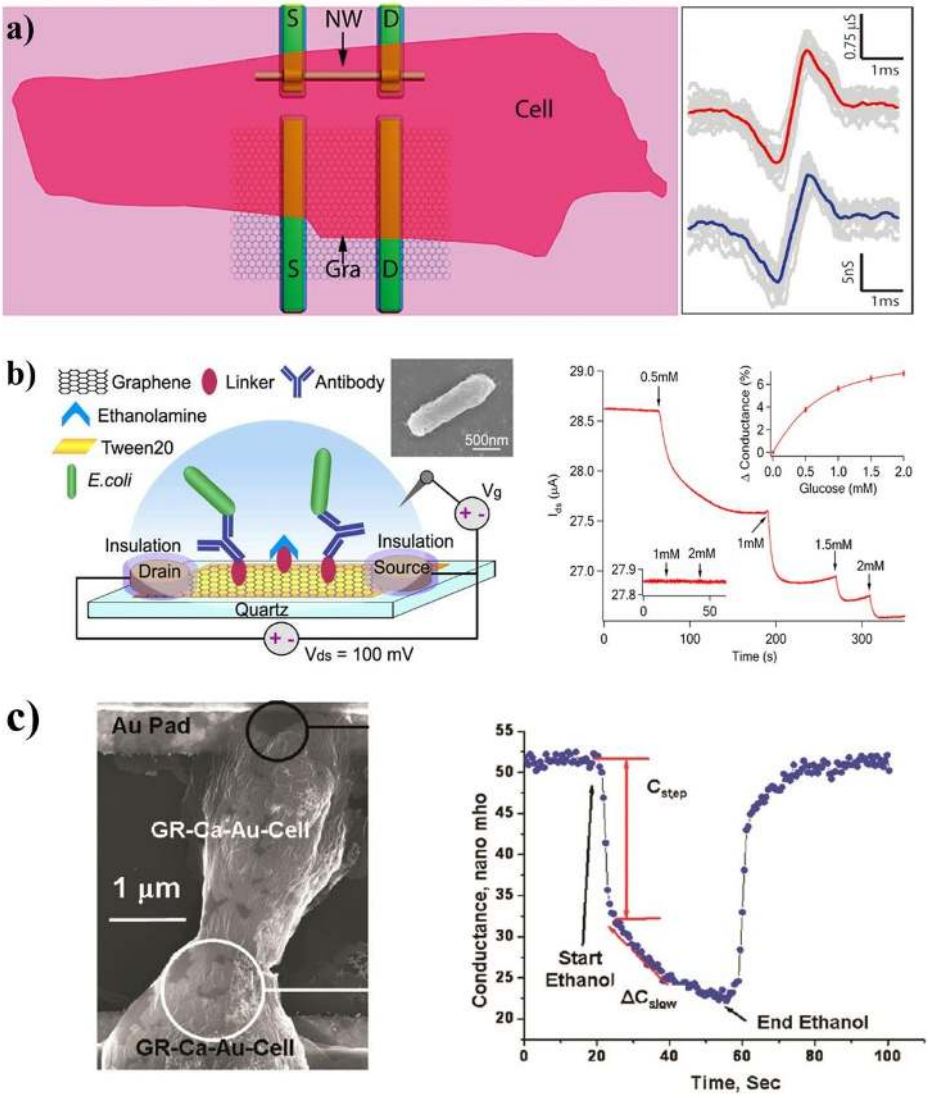


**Figure 7.** Electronic graphene sensors for cellular detection. (a) Detection of cellular bioelectricity. Left: Representation of a cardiomyocyte cell interfaced to a graphene-FET and a sillicon nanowire-FET device; Right: thirteen electrical signals (gray traces) from the graphene-FET (upper data) and the silicon nanowire-FET (lower data) devices in response to the spontaneous action potentials produced by the cardiomyocyte. The peaks were aligned in time and the average was plotted in red and blue, respectively. Adapted from ref 235. Copyright 2010 American Chemical Society. (b) Detecting bacteria and their metabolic activity. Left: Illustration of anti-E.coli antibody functionalized graphene-FET for detection of E.coli. Inset: Scanning electron microscopy (SEM) image of an *E. coli* on antibody functionalized CVD-graphene. Right: Real-time current recording ($V_{ds}$=100 mV and $V_g$=0V) of a

bacteria-bound graphene device with application of glucose at different concentrations. Lower inset: bacteria free graphene sensor was not responsive to glucose. Upper inset: Percentage change in graphene conductance versus glucose concentration. Adapted from ref 105 Copyright 2011 the Royal Society of Chemistry. (c) Electromechanical interface between graphene and yeast cell. Left: SEM image showing two RGO covered yeast cells spanning the gap between Au electrodes. GR = RGO. Right: Real-time recording of the conductance change of the RGO layer on cell (biased at 100 mV) when the yeast cell was exposed to ethanol (99%) for 40 s. A reversible drop in conductance was observed. Adapted from ref 240. Copyright 2011 American Chemical Society.

### 5.5 Cellular detection

In recent years, nanoelectronic biosensors based on 1D semiconducting nanostructures (carbon nanotubes and silicon nanowires) have been coupled with live cells to detect their low presence and dynamic activities.[140, 179-181, 229-231] Owing to its unique properties, graphene adds a new dimension to the nanoelectronics-cell interface. As cell membrane is also a 2D structure (5-nm-thick lipid bilayer), it can intimately interact with flat graphene. In contrast, when cell membrane interfaces with other nanostructures, the interaction may not be tight and homogeneous and the local curvature induced on the thin cell membrane by nanotopographic structures may alter cell functions in intriguing ways.[232] Given the close interaction between the cell membrane and graphene as well as the highly sensitive nature of graphene's electrical properties, the cell-activity-induced local electrical and chemical fluctuations in the nanogap between graphene and cell membrane could significantly change the graphene conductance.

Silicon nanowire[179, 233, 234] and carbon nanotube transistors[229] have been used to detect cellular bioelectricity (action potentials) resulting from the orchestrated activities of membrane ion channels. Lieber and co-works recently demonstrated a graphene FET to extracellularly detect action potentials from single electrogenic cardiomyocytes (Figure 7a).[235] Mechanically exfoliated graphene was used to fabricate devices by e-beam lithography. The authors showed that the sensitivity of graphene FET is superior to conventional metallic microelectrodes and comparable to silicon nanowire FET. The device response is triggered by the field-effect due to the change of electrical potential at the nano-interface between the cell and the FET while the ionic current through the membrane ion channels flows in the resistive solution in the nano-interface. Although the field-effect of graphene is less prominent than silicon nanowire, the comparable signal-to-noise ratio was obtained by graphene FET. This may be attributable to its much larger interfacing area with the cell. It would be interesting to see the performance of graphene nanoribbons (GNRs) with large bandgap in detection of cellular bioelectricity. Supposedly, GNRs are able to provide both high sensitivity because of their prominent field-effect and high spatial resolution because of their nanoscale lateral dimension.

In a work by He *et al.*, centimeter-long, micrometer-wide, ultrathin and continuous RGO network films were made using microfluidic patterning and coupled with neuroendocrine PC12 cells.[236] Such readily fabricated RGO FETs were able to detect rapid vesicular secretion of hormone catecholamines from PC12 cells triggered by membrane depolarization. Catecholamine molecules released into the membrane-FET nanogap interact with RGO sheets through π-π interaction, and increase p-type RGO conductance *via* p-doping. The specificity of detection is achieved in the well-defined biological context, in this case, the highly regulated stimulus-secretion coupling. As compared to electrophysiological single cell recordings[237, 238], this nanoelectronic approach is non-invasive and does not require high experimental skills. As also demonstrated by the authors, microfluidic patterned RGO thin-film devices can be made on flexible substrates that could conform onto a curved target (*e.g.*, an organ).

Coupling between graphene FETs and bacteria has also been demonstrated for detection of the presence and activities of bacteria. The bacteria sensor demonstrated by Mohanty *et al.* used a microsized amine-modified graphene (GA) sheet as the sensing material.[100] The GA was synthesized by either exfoliation of ammonia plasma-treated graphite flakes or exposing GO sheets to hydrogen plasma followed by ammonia or nitrogen plasma. Significant conductance increase was observed upon attachment of single bacterium which imposes prominent p-doping to the GA sheet (ca. ~1400 conducting holes per bacterium). The high sensitivity may be ascribed to the high hole mobility of GA and the firm interaction between the positively charge amino groups on GA and the highly negatively charged bacterial wall. However, this sensor is not practical because the detection relied on non-specific electrostatic adhesion of bacteria without discrimination of bacterial species and the measurement was non-physiologically conducted in dry nitrogen atmosphere.

Chen and co-workers recently demonstrated a CVD-grown graphene based sensor to specifically and sensitively detect *E. coli* bacteria in solution (Figure 7b).[105] Graphene was functionalized with anti-*E. coli* antibodies as the recongintion element, and non-specific attachement of other bacteria species or molecules was prevented by coating of a passivation layer. *E. coli* at a concentration as low as 10 cfu/ml can be detected while a different bacteria species at a much higher concentration cannot produce a signficant signal. The detection is based on the field-effect caused by the highly negatively charged bacterial wall. The detection limit of this graphene sensor is much better than the sensor made with a similarly sized thin-film network of single-walled carbon nanotubes.[239] Furthermore, the authors showed that the graphene FETs are able to detect the glucose induced metabolic activities of the bound *E. coli* bacteria in real time. It was hypothesized that discharge of organic acids (metabolites) into the nano-gap between the graphene and the interfacing bacterial surface decreases the local pH and consequently the graphene conductance.

Electromechanical coupling between graphene and yeast cell was recently reported.[240] In this interesting work, RGO microsheets were coated on the cell surface forming an electrically conductive layer (Figure 7c). By monitoring the electrical conductance of the RGO layer, the dynamic mechanical response of a yeast cell to osmotic stresses or heat shock can be recorded in real-time, because a change in the cell volume leads to straining of the RGO sheets and consequent formation of wrinkles that reduces the electrical conductivity of RGO layer. The ultrathin thickness makes the RGO sheet highly sensitive to structural deformation.[196]

Evidently from the examples discussed in this section,

graphene electronic sensors promise applications in rapid detection of rare pathogenic microbes or pathological cells (*e.g.*, cancer cells), high throughput studies of dynamic cell functions, and high throughput drug screening targeting on those cell functions.

### 5.6 Integrating biomimetic membrane with graphene FET for biosensing

Cell membrane is perplexingly complex, crowed with a huge variety of molecular machines (membrane proteins). To enable the study of membrane protein activities in the simplest native environment, integration of artificial lipid bilayer (biomimetic membrane) with carbon nanotube FETs has been demonstrated.[241, 242] Presumably, the flat and size-tunable graphene is a better alternative to interface with (support) biomimetic membranes for biosensing, in particular, examining the functions of molecules that operate in or on cell membranes, or disrupt cell membranes.

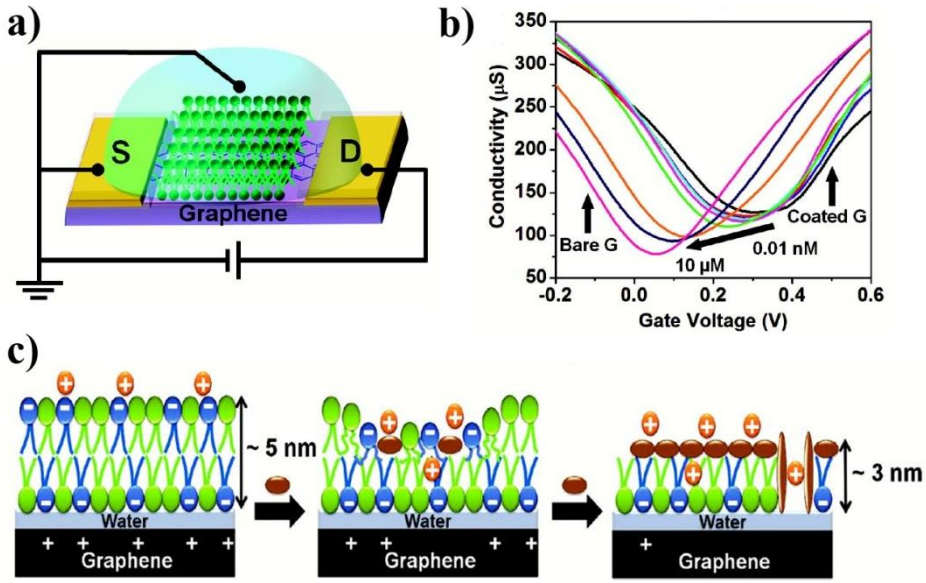


**Figure 8** Integrating biomimetic membrane with graphene FET for biosensing. (a) Schematic representation of biomimetic membrane-CVD grown graphene field-effect transistor. (b) Transfer curves of biomimetic membrane-CVD grown graphene FET with increasing magainin 2 concentrations and (c) Schematic diagram showing sensing concept of membrane thinning effect by magainin 2 (brown ovals). Adapted with permission from ref 243. Copyright 2010 American Chemical Society

Ang *et al.* deposited gram-negative bacteria biomimetic membrane on CVD grown graphene film.[243] And this hybrid device was used to detect magainin 2, which is an antimicrobial agent secreted by skin cells of African frog (Figure 8). Magainin 2 disrupts the thin biomimetic membrane by dislodging the upper layer of the lipid from the surface. The thinning of membrane thickness from ca. 5nm to ca. 3nm reduced the field-effect from the negatively charged lower membrane layer because of the charge screening by the ionic solution within the Debye distance. Low detection limit was achieved at 100 pM with a large Dirac point shift (50 mV). Such graphene sensor opens a new route to study disruptions or functions of cell membranes (*e.g.*, drug cytotoxicity, ligand-receptor interaction, or ion channel activities).

### 5.7 Improving the performance of graphene electronic sensors

Graphene based nanoelectronic sensors are only emerging. Strategies can be devised to further improve their performance. For example, Cheng *et al.* showed that suspending the graphene sheet by etching away the underneath silicon oxide reduces the low-frequency noise originated from the graphene-substrate contact, leading to an improvement of the signal-to-noise by 14 dB for both holes and electron.[244] In addition, since the scattering effect from the substrate is removed, the device sensitivity (transconductance) increases by 1.5-2 times. Dankerl *et al.* have fabricated graphene FET array on epitaxially grown graphene on SiC.[245] Individually addressable graphene FETs in the array could be differentially functionalized for simultaneous detection of multiple targets for high throughput and information-rich analyses. The throughput and performance of graphene electronic sensors may be further improved by the integration with micro/nanofluidics.[246]

Electronic sensors based on a single graphene nanoribbon (GNR) or quantum dot are anticipated to offer high sensitivity and high spatial resolution. As an example, Min *et al.* theoretically demonstrated a GNR based DNA sequencing device, in which a GNR is suspended on top of a fluidic nanochannel.[247] When a ssDNA is electrophoretically threaded through the nanochannel, electrical signatures of four types of nucleotides can be resolved because 1) the narrow width of GNR is comparable to the size of a base and 2) the ballistic conductance of GNR diminishes at specific energies corresponding to the characteristic π-molecular orbitals *via* Fano resonance. The authors also argued that narrow GNRs are superior to carbon nanotubes whose multiple

conductance levels and multiple stacking reduce the characteristic electrical perturbations by the bases over the noise level. Recently, Dong *et al*.[248] showed that the network of RGO nanoribons obtained by chemically unzipping multiwalled carbon nanotubes exhibits higher on/off ratio than graphene or rGO film and a significantly higher sensitivity in electrically detecting adenosine triphosphate (ATP) molecules as compared to that of single-walled carbon nanotube (SWCNT) network. [249]

Use of smaller recognition elements (*e.g.*, antigen-binding fragment of antibodies) to bring the targets closer to graphene should also enhance the sensitivity. As a novel alternative, artificial receptors could be created on graphene using molecular imprinting (MIP),[250] which involves polymerization around the template (target) molecules and subsequent wash-away of the templates (leaving the artificial or synthetic binding sites open for the specific binding with the target molecules). MIP has been employed for carbon nanotube based biosensors.[251] We speculate that flat graphene sheet is more suitable for uniform and effective MIP in comparison with small nanotubes. Such artificial receptors ensure direct contact between the graphene and the targets, high specificity, and robustness.

## 6 Optical Sensors

Graphene oxides exhibit interesting optical properties.[61] Unlike zero-gap graphene or other carbonaceous materials, GO can fluoresce in a wide range of wavelength (from near-infrared to ultraviolet)[252]. This is because the disordered oxygenated functional groups on GO confine π electrons within the $sp^2$-carbon nanodomains, thereby giving rise to a local energy gap that inversely scales with the domain size. Therefore, GO has the potential to serve as a universal fluorescence label for optical imaging.[253] Interestingly, just like other graphitic materials, GO is also capable of quenching fluorescence.[254] The quenching efficiency of GO is superior to the conventional organic quenchers. It has been shown that quenching even at a distance of 30 nm is attainable by GO.[255] On the basis of its fluorescence and quenching abilities, GO can serve as either an energy donor or acceptor in a fluorescence resonance energy transfer (FRET) sensor. The optical characteristics (*e.g.*, fluorescence wavelength and quenching efficiency) of GO is tunable by controlling the extent and type of its oxygenation.[255-257]

Graphene materials may also assist to enhance the performance of optical sensors, by increasing signal-to-noise ratio, loading of recognition element, adsorption of the target molecules, efficiency of signal transduction, etc. For example, taking advantage of their quenching properties, graphene materials can be used to reduce fluorescence interference in Raman spectroscopy[258] and enhance the Raman signal through charge transfer with the adsorbed molecules.[259] Other merits of graphene materials (GO in particular) may also be useful for optical sensors, such as, high optical transparency, high surface-to-volume ratio, the ability to intimately interact with many molecules *via* π-π or electrostatic or hydrophobic interaction, the ability to catalyze luminescence-generating or signal-transduction reaction, and so on.

### 6.1 As the sensing element in FRET

GO based FRET sensors may consist of three components: a recognition probe (*e.g.*, probe ssDNA that hybridizes with target ssDNA, or aptamer - an oligonucleic acid that binds with specific target molecule), a reporter fluorophore conjugated on the probe, and GO. Initially, the fluorescently tagged probes attach firmly onto GO through strong π-π interaction between nucleobases and GO plane. The close interaction leads to fluorescence quenching. Binding of the detection targets then causes conformational change of the probe, which, in turn, leads to dissociation of the probe from GO surface. And the subsequent termination of FRET restores the fluorescence of the initially quenched fluorophores. This kind of mix-and-detect sensors is convenient and cheap. Tang *et al.* reported such a GO based fluorescence quenching-recovery sensor to detect ssDNA with a LOD of nM range.[260] The authors also showed that their sensors can perform even in presence of DNAase because ssDNA detained on GO surface was found to be indigestible by DNAase. Two similar DNA sensors, which are also able to distinguish single-base-mismatch, have also been demonstrated.[261, 262]

Cite this: DOI: 10.1039/c0xx00000x

www.rsc.org/xxxxxx

ARTICLE TYPE

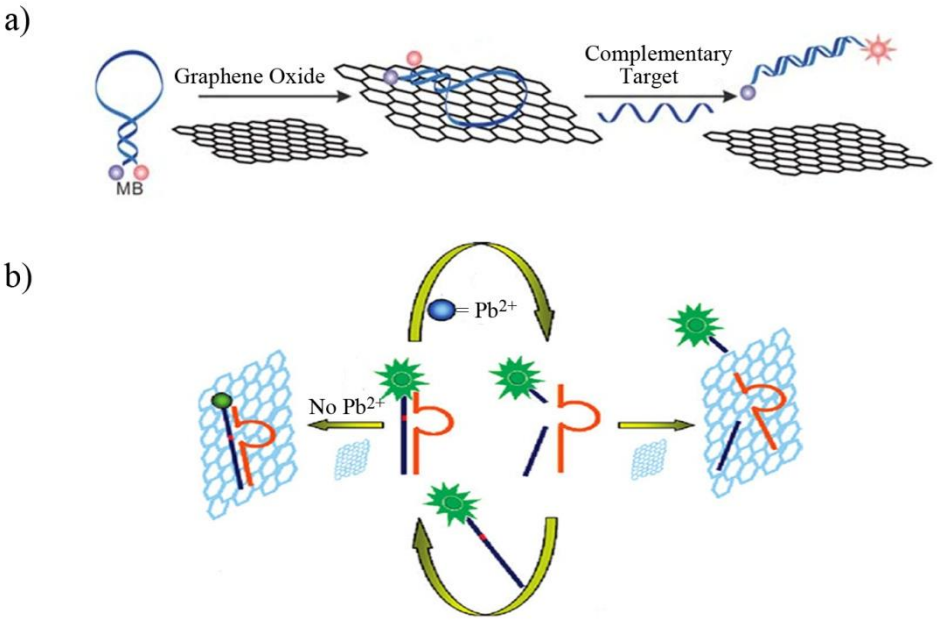


**Figure 9**. GO as the quencher in FRET sensor. (a) Schematic illustration of DNA hybridization using a double-quenching system consisting of GO and molecular beacon (MB). Adapted with permission from ref 263. Copyright 2010 the Royal Society of Chemistry (b) schematic illustration of the DNAzyme-GO based fluorescence sensor for detection of $Pb^{2+}$. Adapted with permission from ref 281. Copyright 2011 American Chemical Society

In order to further improve the sensitivity, Li *et al.* designed a double-quenching system combining GO and molecular beacon (MB - a hairpin-structured oligonucleotide conjugated with a FRET pair) (Figure 9a).[263] Relief of both GO quenching and intra-probe quenching of MB upon binding of the complementary DNAs greatly enhances the signal-to-noise ratio, resulting in a low LOD of 0.1 nM. Due to the high thermal stability of MB-GO complex, this sensor can operate at a high temperature (75℃), promising its use in polymer chain reaction (PCR). Alternatively, Dong *et al.* employed CdTe quantum dot (QD) as the fluorescence reporter to construct GO/MB-QD sensing platform.[264] The mercaptoacetic acid (MPA)-capped CdTe QD was served as a core for adsorption of multiple MBs to form a probe complex. It is worth mentioning that, compared with commonly used organic fluorophores, QD possesses many advantages including high quantum yield, high photostability, and size-tunable absorption and emission.[265]

Using similar detection scheme and particularly designed aptamer receptors, proteins and metal ions have also been detected. Based on GO-aptamer system, Lu *et al.* devised a human thrombin sensor with a nM detection limit,[266] which excels regular dye-quencher pair labeled aptamers[267] and comparable to aptamer-CNT based optical sensors.[268] Another thrombin sensor with a lower detection limit (pM level) was demonstrated, using surfactant dispersed RGO instead of GO.[269] A GO-FRET sensor to detect Cyclin A2 - an early-stage cancer indicator has been shown.[270] The achieved LOD of 0.5 nM is 10-fold lower than that of SWCNT based sensors. Notably, for the first time, Wang *et al.* reported an intracellular molecular sensor using GO-FRET scheme for detection of intracellular ATP molecules.[271] They showed that GO nanosheets (~100 nm) attached with fluorescent ATP-specific aptamers can be readily uptaken by the mice epithelial cells without introducing apparent cytotoxicity, because of the small size, high solubility, and biocompatability of GO nanosheets. In addition, in agreement with a previous observation ,[260] the GO sheets also protect the aptamer probes from being cleaved by the intracellular enzymes.

Wen *et al.* developed an $Ag^+$ sensor with a LOD of 5 nM by employing fluorescence labelled $Ag^+$-specific aptamer (cytosine-rich oligonucleotide) as the probe.[272] Association of $Ag^+$ ions with the cytosine bases induces the conformational change of the probe and yields a rigid hairpin structure. This leads to an increase of the distance between the GO sheet and the fluorophore beyond the effective quenching region, hence, termination of FRET. In the practical tests of river water, the sensor exhibits excellent specificity against various interferences (*e.g.* other ion species and particles) and its LOD satisfies the requirement of US Environmental Protection Agency (EPA) for drinking water.

FRET sensors with different detection schemes have been explored. For example, He *et al.* demonstrated a DNA sensor by using 'post-mixing method', in which fluorescent probe-ssDNAs were first mixed with target-ssDNAs followed by addition of GO sheets.[273] Because the fluorescence of the unhybridized probes is effectively quenched by GO sheets, the remained fluorescence intensity from the hybridized probes indicates the concentration

of target DNAs. Using this post-mixing method, the reaction time is largely reduced due to the absence of competition between the interaction of GO/probe DNA and the interaction of probe DNA/target DNA. Furthermore, in this study, different probe DNAs with distinctly coloured fluorophores were co-decorated on GO sheets in order to simultaneously detect multiple DNA targets. The interference between different probe DNAs was found to be negligible. The detection limit of such multicoloured DNA sensors can reach as low as 100 pM. It outperforms the previously reported FRET sensors based on molecular beacons[274, 275] or other nanomaterials.[276, 277]

Instead of using ssDNA or apatmer as the recognition element, Balapanuru *et al.* used organic dye 4-(1-pyrenylvinyl)-N-butylpyridinium cation ($PNP^+$) as the probe for dsDNA.[278] Electrostatic interaction between negatively charged dsDNAs and positively charged $PNP^+$ is able to remove $PNP^+$ from GO surface and cause quench recovery. Cai *et al.* used butterfly-shaped conjugated oligoelectrolyte as the FRET donor and receptor to specifically detect heparin (a glycosaminoglycan).[279] Using a upconverting phophors (UCP) as the donor and conjugated concanavalin A as the receptor, a GO-FRET sensor was developed for detection of glucose in human serum samples.[280] In a novel work by Zhao *et al.*, a GO-FRET sensor for detection of $Pb^{2+}$ ions was developed using the hybrid of DNAzyme and fluorescence labelled substrate DNA as the recognition element (Figure 9b).[281] The DNAzyme-substrate DNA complex was brought onto GO surface *via* π-π interaction between GO and the large loop sequence on DNAzyme. Once $Pb^{2+}$ is introduced, it activates the DNAzyme to cleave the substrate strand into two parts, releasing a short fluorophore-linked oligonuleotide fragment which is too short to attach back onto GO again. Consequently, the fluorescence is recovered from quenching. The reaction also releases DNAzyme from the GO surface, allowing it to hybridize with another bound substrate DNA and thus providing an amplified signal for $Pb^{2+}$ detection. This sensor is able to detect $Pb^{2+}$ at a concentration as low as 300 pM with a selectivity 2 orders higher than other heavy metal ions. The similar strategy was used by Wen *et al.*[282] Based on the finding that $Pb^{2+}$ could specifically modulate the interaction between GO and a $Pb^{2+}$ dependent 8-17 DNAzyme *via* cleavage of 17S substrate, a simple mix-and-detect $Pb^{2+}$ sensor was developed. In the presence of $Pb^{2+}$, the substrate DNA strand is specifically and irreversibly cleaved at cleavage site of 17S substrate, resulting in the disassembly of the duplex DNAzyme into three ssDNA fragments: the 3'- and 5'- fragments of substrate strand and the enzyme strand. These ssDNAs could be adsorbed onto GO nanosheets *via* π-π stacking between the bases and the aromatic structure of GO and consequently the dye modified DNAs were quenched. This $Pb^{2+}$ sensor gives a LOD of 0.5 nM.

Instead of using GO as the FRET quencher, Liu and colleagues used GO as the energy donor in their FRET sensor for detection of ssDNA.[283] Gold nanoparticles (AuNPs), which served as the energy acceptor (fluorescence quencher), were conjugated on the target ssDNA. When the target ssDNA hybridizes with the probe DNA covalently linked on GO surface, AuNP brought onto GO surface quenches the fluorescence of GO. Using similar AuNP quenching scheme, a sensor for detection of rotavirus was also demonstrated (Figure 10).[284] Firstly, rotavirus-specific antibodies were covalently immobilized on GO surface. After rotaviruses were fetched by the antibodies, the complex of the secondary rotavirus-antibody /DNA/AuNP were added to form a sandwich structure, causing quenching of GO fluorescence by AuNPs. This immune-pathogen sensor with high selectivity, sensitivity (~1000 pfu/ml) and rapid detection time could be a promising alternative to the conventional time-consuming pathogen detection methods.

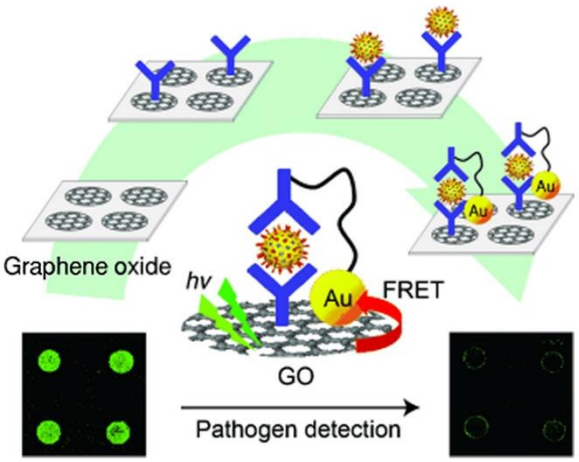


**Figure 10**. GO as the fluorescence donor in FRET sensor for immunodetection of pathogen. Adapted with permission from ref 284. Copyright 2010 Wiley-VCH Verlag GmbH & Co. KGaA, Weinheim

### 6.2 As a facilitator in optical sensors

Instead of serving as the (or a part of) sensing element, graphene materials may also be used to improve the performance of optical sensors. Wu *et al.* theoretically proposed that graphene can improve the performance of surface plasmon resonance (SPR) based biosensors.[285] Firstly, the coated graphene can enhance adsorption of biomolecules onto the metal/dielectric interface at which surface electromagnetic wave propagates. Secondly, multi-graphene layers can increase the sensitivity of SPR response. Choi *et al.* also theoretically demonstrate that graphene-on-silver substrate can enhance the SPR sensitivity by 3 times in comparison with the conventional gold-film-based SPR biosensor.[286] In addition, graphene can prevent oxidation of silver due to its high impermeability to oxygen. Wang *et al.* fabricated a label-free, regenerative and sensitive SPR sensor to detect α-thrombin with an ultralow detection limit of 50 pM.[287] The thrombin aptamer (TBA) is noncovalently adsorbed on the RGO layer, which is assembled on a positively charged SPR Au (p-Au) film *via* electrostatic interaction. When TBA fetches the target molecule (α-thrombin), it detaches from the RGO, producing an obvious SPR angle decrease. The authors also illustrated that such SPR sensor exhibit excellent selectivity and can be applied in real biological fluid (1% pretreated human plasma).

$Cd^{2+}$ can be detected based on absorbance change upon its binding with 5,10,15,20-tetrakis (1-methyl-4-pyridinio) porphyrin (TMPyP). It has been demonstrated that RGO can accelerate this binding reaction by 150 times because RGO sheets are able to flatten TMPyP through electrostatic and the π-π interaction with porphyrin rings on TMPyP and facilitate the coordination reaction between $Cd^{2+}$ ions and TMPyP.[288] Glucose can be

detected based on absorbance change of 3,3,5,5-tetramethylbenzidine (TMB) when it is oxidized by $H_2O_2$ - the product of glucose oxidation by glucose oxidase. Song *et al.* showed that COOH-GO, which was synthesized by adding NaOH and chloroaceticacid into GO suspension, exhibits intrinsic peroxidase catalytic activity (higher than that of horseradish peroxidise); and COOH-GO can serve as an intermediate to transfer electrons from TMB to $H_2O_2$.[289] High catalytic activity, high affinity to organic substrates, ease of preparation, low-cost and excellent stability makes COOH-GO a better choice to facilitate TMB based glucose detection, compared with other peroxidases (*e.g.*, horseradish peroxidise or $Fe_3O_4$ nanoparticles).

In an electrochemiluminescence sensor for detection of glutathione (a cellular antioxidant), GO sheets were added in the solution to amplify electrogenerated chemiluminescence (ECL) by facilitating the generation of quantum dot radicals and oxygen radicals.[290] The authors argued that GO with a wide range of energy bandgaps serves as a good intermedium for electron transfer. The sensor, with a LOD of 8.3 μM, was successfully employed to assess real samples (glutathione-containing eye drug). In an ECL sensor for detection of prostate protein antigen (prostate cancer marker), RGO sheets were used as the electrode material to enhance the ECL reaction taking advantage of its excellent electrocatalytic and conductive properties.[291]

In the work by Lu *et al.*, silver nanoparticle (Ag NP) decorated RGO film was used as the substrate for surface enhanced Raman scattering (SERS) to detect aromatic molecules. [292] A LOD of nM was obtained because of the ability of RGO to enhance Raman signal and quench the fluorescence background and the high adsorption efficiency of RGO towards aromatic compounds. Ren *et al.* reported a SERS sensor for detection of folic acid molecules. [293] PDDA-functionalized GO and AgNPs was used as the substrate and a low LOD of 9 nM was attained in both water and diluted human serum.

## 7. Nanopore sensors

A nanopore, which resides on an insulating membrane and has a molecular diameter, can be used as a molecular detector with exquisite (single molecule or even intra-molecular) sensitivity. When a molecule passes through a narrow pore that connects two separated electrolyte solutions, the ionic current flowing through the pore is partially blocked, producing a current signature influenced by the charge state and subtle molecular structure of the occupying molecule or its segment. Protein nanopores embedded within a lipid bilayer have been used first for detection of DNA and RNA molecules.[294] And the discovery that the base composition of DNA/RNA molecule affects the signal of current blockage[295] has invited tremendous interests in developing nanopore-based ultra-fast DNA sequencing techniques. To overcome the poor stability and durability of biological nanopores, solid-state nanopores created on dielectric membranes (*e.g.*, $Si_3N_4$ or $SiO_2$) have been developed.[296, 297] However, an essential requirement for nanopores to achieve single-base sensitivity for DNA sequencing is that the nanopore membrane has to be thinner than or as thin as the distance between the two successive bases (0.34 nm which is about an atom apart). This is much smaller than the thickness of lipid bilayer (~5 nm) and the currently achievable thickness of dielectric membranes. Graphene, the thinnest material known in the world, makes nanopore-sequencing an attainable possibility. In addition, the extraordinary mechanical stiffness and chemical stability of graphene assure the manufacturability and durability of a free-standing graphene film with created nanopore(s).

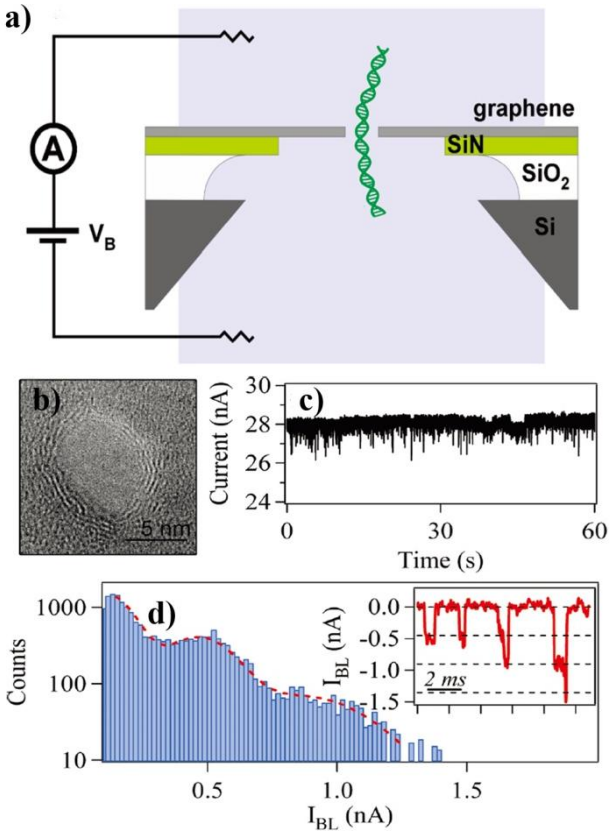


**Figure 11.** Graphene nanopore for detection of single DNA molecule. (a) Illustration of few-layer graphene (1-5 nm thick) suspended over a 1 $\mu$m diameter hole in a 40 nm thick silicon nitride (SiN) membrane. The SiN membrane is suspended over an approximately 50 × 50 $\mu m^2$ aperture in a silicon chip coated with a 5 $\mu$m $SiO_2$ layer. The device is inserted into a PDMS measurement cell with microfluidic channels that form reservoirs in contact with either side of the chip. A bias voltage, $V_B$, is applied between the reservoirs to drive DNA through the nanopore. (b) TEM image of an ~8 nm graphene nanopore. (c) DNA translocation events as signaled by discrete ionic current blockages. (d) Histogram of blocked currents for measured translocation events for the device at $V_B$ = 100 mV in 1 M KCl solution. Data are fit using two Gaussian functions with mean values at 0.45 and 0.90 nA. Inset displays concatenated events caused by unfolded or folded translocating DNA molecules. Blocked current signal ($I_{BL}$) values of 0.45, 0.9, and 1.35 nA are indicated with dashed black lines, indicating unfolded, singly folded, and doubly folded entries, respectively. Adapted with permission from ref 298. Copyright 2010 American Chemical Society.

Using electron beam drilling, Merchant *et al.* fabricated a nanopore (5 – 10 nm in diameter) on CVD-grown few-layered graphene sheet (3-5 layers), which was suspended on a micrometer-hole on silicon nitride membrane (Figure 11).[298] In addition, a titanium dioxide nanolayer was coated on graphene surface to make a cleaner and more wettable pore, and consequently, to reduce the current noise.[296] However, this comes with a price of increased pore thickness. To reduce the thickness

of graphene nanopore, Schneider *et al.* used a single-layered and un-coated graphene sheet obtained from mechanical exfoliation[299] and Garaj *et al.* used one- or double-layered CVD grown graphene.[300] The graphene nanopores produce a larger current blockage upon DNA translocation than that from the conventional solid-state nanopores because of the ultrathin nature of the graphene nanopores. And despite its atomic thickness, graphene is a remarkable ionic insulator.

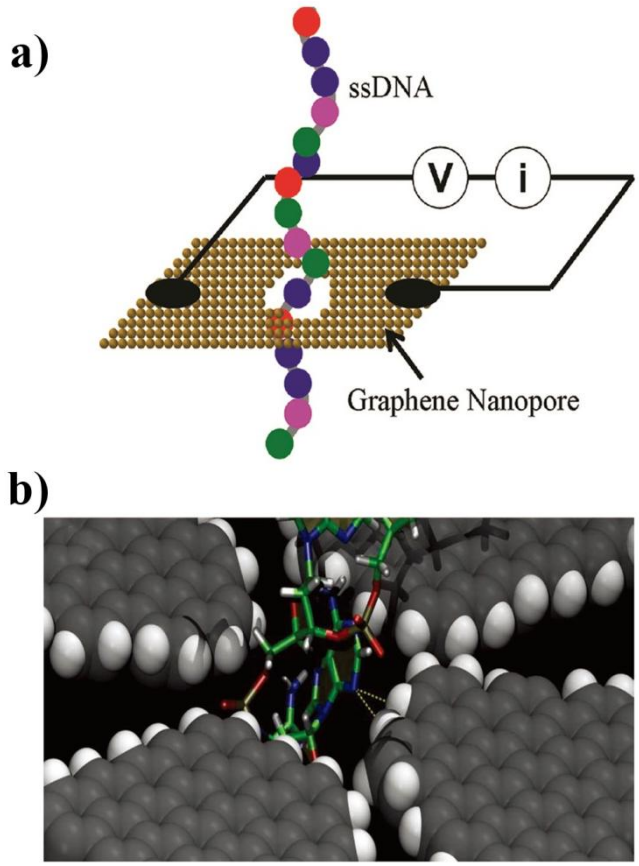


**Figure 12.** Graphene nanopore for rapid DNA sequencing. a) Illustration of translocation of a ssDNA through a graphene nanopore while the electronic current in graphene is monitored. Adapted with permission from ref 302. Copyright 2010 American Chemical Society. (b) Snapshot extracted from the molecular dynamics simulation of ssDNA translocation through a graphene nanopore, showing a moment when two H-bonds (dotted yellow lines) are formed simultaneously between the nitrogen atom of a DNA nucleobase and two H atoms attached to the graphene-edge. Adapted with permission from ref 305. Copyright 2011 WILEY-VCH Verlag GmbH & Co. KGaA, Weinheim.

Although graphene nanopores promise for spatially-resolved detection of individual nucleotides, they just like other nanopores still face several challenges in order to practically realize DNA sequencing. These include fast translocation velocity of DNA driven by the intense electrical field, low bandwidth in recording of ionic-current, low signal magnitude due to slow mobility of ions and blockage based detection scheme [301]. Nelson *et al.* proposed a graphene nanopore drilled on graphene nanoribbon (GNR) FET (Figure 12a).[302] They demonstrated theoretically that when ssDNA is traveling through the nanopore, the GNR conductance changes due to modulation in current tunneling across the pore and the field-effect due to electrostatic interaction of the nucleotide with the ribbon. Different types of nucleotides can be distinguished due to their characteristic energy levels and characteristic interactions with nanoribbon, suggesting the feasibility of rapid DNA sequencing. The signal response from such electronic-conductance-based nanopore sensor is several orders higher that the ionic-current-based nanopore sensors (mA vs. nA). The high sensitivity is attributable to the new sensing mechanism, high carrier mobility of graphene, and large energy bandgap provided by GNR. In another study, it was argued that the sensitivity could be further improved if the nanopore is created at the edge of the GNR in order to take advantage of its edge-sensitivity.[303]

It has been theoretically proven that a graphene nanogap (gap width ~1.0 - 1.5 nm) can be used to electrically read the base sequence of a single DNA molecule based on change of tunneling current across the gap, which is sensitive to the characteristic local electronic densities of different nucleotides.[304] Inspired by this idea, He *et al.* proposed a graphene nanopore defined by four graphene nanoelectrodes, which may be fabricated by e-beam etching on a graphene film deposited on a thin substrate (Figure 12b).[305] Transverse tunneling conductance is recorded between two opposite nanoelectrodes when an ssDNA is electrophoretically driven through the nanopore. The hydrogenated edges of the four electrodes couple with the DNA base *via* hydrogen bond, which slows down the DNA translocation velocity and enhances the electron tunneling rate over vacuum tunneling. The hydrogen bonding thus can increase the average transverse conductivity by about 3 orders of magnitude with reduced statistical variance. With novel design on pore formation[306] and functionalization,[307] graphene nanopore techniques would advance further for DNA sequencing or single molecule characterization in general.

## 8. Conclusions and Outlook

In spite of its very short history, graphene has already demonstrated great successes in biological and chemical sensing. Because of the availability of a spectrum of graphene materials and their pluripotent sensing capabilities, graphene based sensors have already been employed for a dazzling diversity of targets ranging from gaseous molecules, small chemicals and ions, biological molecules (*e.g.*, sugars, proteins, DNAs), bacterial and animal cells, as well as dynamic cellular activities. These sensors exhibit outstanding performance as compared with the state-of-the-art techniques, in terms of sensitivity, selectivity, detection range, temporal resolution, reproducibility, response time, or cost. Although most of these developments are merely proof-of-concept demonstrations, as a step forward to the practical or commercialized uses, some of them have been proven to be functional for complex real samples, for example, serum samples. Without a doubt, the full potential of graphene based sensors is far from being reached. Some graphene materials (*e.g.*, GNR, graphene QD, bilayered graphene) have barely been explored for sensor applications so far, although their potentials are highly anticipated due to their exceptional properties. And new graphene materials and structures are still emerging, for instances, graphane (a hydrognenated twin material of graphene)[308] and CVD-grown three-dimensional graphene foam.[309] Hybridizing or compositing graphene materials with various organic and inorganic systems (such as, polymers, carbon nanotubes, nanoparticles)[108, 309-312] are also extending the arsenal for graphene sensor development. By combing its different capabilities and merits, a graphene sensor that is equipped with

multiple sensing modalities (*e.g.*, electronic and optical) shall be possible. And a graphene sensor that is able to detect single biomolecule shall not be far-reaching. Taken together, the abilities and applications of graphene sensors are only limited by imagination.

Currently, the development and wide-spread application of graphene sensors are largely hindered by the lack of methods for controllable, reproducible, scalable, and facile preparation of graphene materials with defined structures and properties.[67] In addition, better understandings on graphene properties, the interactions between graphene and molecules/cells, and the detection (or signal transduction) mechanisms are critical. To move forward, the collaborations between different disciplines and technologies are necessary. In witness of its current explosive development, we envision that the emerging graphene sensors would soon bring significant impacts on environmental and safety monitoring, diagnosis, biological studies, and drug screening.

## References


1. D. S. L. Abergel, V. Apalkov, J. Berashevich, K. Ziegler and T. Chakraborty, *Advances in Physics*, 2010, **59**, 261-482.
2. M. J. Allen, V. C. Tung and R. B. Kaner, *Chemical Reviews*, 2010, **110**, 132-145.
3. M. F. Craciun, S. Russo, M. Yamamoto and S. Tarucha, *Nano Today*, 2011, **6**, 42-60.
4. C. N. R. Rao, K. Biswas, K. S. Subrahmanyam and A. Govindaraj, *Journal of Materials Chemistry*, 2009, **19**, 2457-2469.
5. V. Singh, D. Joung, L. Zhai, S. Das, S. I. Khondaker and S. Seal, *Progress in Materials Science*, 2011, **56**, 1178-1271.
6. Y. M. Lin, K. Jenkins, D. Farmer, A. Valdes-Garcia, P. Avouris, C. Y. Sung, H. Y. Chiu, B. Ek and Ieee, *Development of Graphene FETs for High Frequency Electronics*, 2009.
7. F. S. F. Schwierz, *Nature Nanotechnology*, 2010, **5**, 487-496.
8. J. S. Wu, W. Pisula and K. Mullen, *Chemical Reviews*, 2007, **107**, 718-747.
9. Y. Q. Sun, Q. O. Wu and G. Q. Shi, *Energy & Environmental Science*, 2011, **4**, 1113-1132.
10. D. A. C. Brownson, D. K. Kampouris and C. E. Banks, *Journal of Power Sources*, 2011, **196**, 4873-4885.
11. C. K. Huang, Y. X. Ou, Y. Q. Bie, Q. Zhao and D. P. Yu, *Applied Physics Letters*, 2011, **98**, 263104
12. Z. S. Wu, S. F. Pei, W. C. Ren, D. M. Tang, L. B. Gao, B. L. Liu, F. Li, C. Liu and H. M. Cheng, *Adv. Mater.*, 2009, **21**, 1756-1760.
13. J. K. Wassei and R. B. Kaner, *Materials Today*, 2010, **13**, 52-59.
14. Y. X. Huang and P. Chen, *Adv. Mater.*, 2010, **22**, 2818-2823.
15. T. Asefa, C. T. Duncan and K. K. Sharma, *Analyst*, 2009, **134**, 1980-1990.
16. Y. X. Huang, D. Cai and P. Chen, *Analytical Chemistry*, 2011, **83**, 4393-4406.
17. S. Roy and Z. Q. Gao, *Nano Today*, 2009, **4**, 318-334.
18. M. F. Frasco and N. Chaniotakis, *Sensors*, 2009, **9**, 7266-7286.
19. C. P. Han and H. B. Li, *Analytical and Bioanalytical Chemistry*, 2010, **397**, 1437-1444.
20. H. Haick, *Journal of Physics D-Applied Physics*, 2007, **40**, 7173-7186.
21. X. L. Luo, A. Morrin, A. J. Killard and M. R. Smyth, *Electroanalysis*, 2006, **18**, 319-326.
22. K. I. Chen, B. R. Li and Y. T. Chen, *Nano Today*, 2011, **6**, 131-154.
23. F. Patolsky, G. Zheng and C. M. Lieber, *Nanomedicine*, 2006, **1**, 51-65.
24. N. S. Ramgir, Y. Yang and M. Zacharias, *Small*, 2010, **6**, 1705-1722.
25. A. K. Wanekaya, W. Chen, N. V. Myung and A. Mulchandani, *Electroanalysis*, 2006, **18**, 533-550.
26. C. B. Jacobs, M. J. Peairs and B. J. Venton, *Analytica Chimica Acta*, 2010, **662**, 105-127.
27. K. Maehashi and K. Matsumoto, *Sensors*, 2009, **9**, 5368-5378.
28. N. Sinha, J. Z. Ma and J. T. W. Yeow, *Journal of Nanoscience and Nanotechnology*, 2006, **6**, 573-590.
29. T. Zhang, S. Mubeen, N. V. Myung and M. A. Deshusses, *Nanotechnology*, 2008, **19**, 332001.
30. K. S. Novoselov, A. K. Geim, S. V. Morozov, D. Jiang, Y. Zhang, S. V. Dubonos, I. V. Grigorieva and A. A. Firsov, *Science*, 2004, **306**, 666-669.
31. F. N. Xia, T. Mueller, R. Golizadeh-Mojarad, M. Freitag, Y. M. Lin, J. Tsang, V. Perebeinos and P. Avouris, *Nano Letters*, 2009, **9**, 1039-1044.
32. S. Pisana, P. M. Braganca, E. E. Marinero and B. A. Gurney, *Ieee Transactions on Magnetics*, 2010, **46**, 1910-1913.
33. B. Arash, Q. Wang and W. H. Duan, *Physics Letters A*, 2011, **375**, 2411-2415.
34. A. Sakhaee-Pour, M. T. Ahmadian and A. Vafai, *Solid State Communications*, 2008, **145**, 168-172.
35. Y. Wang, R. Yang, Z. W. Shi, L. C. Zhang, D. X. Shi, E. Wang and G. Y. Zhang, *Acs Nano*, 2011, **5**, 3645-3650.
36. A. K. Geim and K. S. Novoselov, *Nat Mater*, 2007, **6**, 183-191.
37. Y. Zhang, Y.-W. Tan, H. L. Stormer and P. Kim, *Nature*, 2005, **438**, 201-204.
38. F. Schedin, A. K. Geim, S. V. Morozov, E. W. Hill, P. Blake, M. I. Katsnelson and K. S. Novoselov, *Nature Materials*, 2007, **6**, 652-655.
39. Y. M. Lin and P. Avouris, *Nano Letters*, 2008, **8**, 2119-2125.
40. A. N. Pal and A. Ghosh, *Applied Physics Letters*, 2009, **95**, 082105
41. W. C. Ren, L. B. Gao, L. P. Ma and H. M. Cheng, *New Carbon Mater.*, 2011, **26**, 71-80.
42. X. C. Dong, P. Wang, W. J. Fang, C. Y. Su, Y. H. Chen, L. J. Li, W. Huang and P. Chen, *Carbon*, 2011, **49**, 3672-3678.
43. A. Reina, X. T. Jia, J. Ho, D. Nezich, H. B. Son, V. Bulovic, M. S. Dresselhaus and J. Kong, *Nano Letters*, 2009, **9**, 30-35.
44. X. S. Li, W. W. Cai, J. H. An, S. Kim, J. Nah, D. X. Yang, R. Piner, A. Velamakanni, I. Jung, E. Tutuc, S. K. Banerjee, L. Colombo and R. S. Ruoff, *Science*, 2009, **324**, 1312-1314.
45. C. M. C. Mattevi, H. Kim and M. Chhowalla, *Journal of Materials Chemistry*, 2011, **21**, 3324-3334.
46. J. Hass, W. A. de Heer and E. H. Conrad, *Journal of Physics-Condensed Matter*, 2008, **20**, 323202
47. J. Kedzierski, P. L. Hsu, P. Healey, P. W. Wyatt, C. L. Keast, M. Sprinkle, C. Berger and W. A. de Heer, *Ieee Transactions on Electron Devices*, 2008, **55**, 2078-2085.
48. S. Y. Zhou, G. H. Gweon, A. V. Fedorov, P. N. First, W. A. de Heer, D. H. Lee, F. Guinea, A. H. Castro Neto and A. Lanzara, *Nat Mater*, 2007, **6**, 770-775.

49. H. P. Boehm, Clauss, A., Fischer, G.O., Hofmann, U, *Z. Naturforsch*, 1962, **17**, 150-153.
50. D. R. Dreyer, S. Park, C. W. Bielawski and R. S. Ruoff, *Chemical Society Reviews*, 2010, **39**, 228-240.
51. C. D. Zangmeister, *Chemistry of Materials*, 2010, **22**, 5625-5629.
52. L. J. Cote, R. Cruz-Silva and J. X. Huang, *Journal of the American Chemical Society*, 2009, **131**, 11027-11032.
53. Y. Y. Shao, J. Wang, M. Engelhard, C. M. Wang and Y. H. Lin, *Journal of Materials Chemistry*, 2010, **20**, 743-748.
54. O. C. Compton and S. T. Nguyen, *Small*, 2010, **6**, 711-723.
55. Q. Y. He, S. X. Wu, S. Gao, X. H. Cao, Z. Y. Yin, H. Li, P. Chen and H. Zhang, *Acs Nano*, 2011, **5**, 5038-5044.
56. M. Pumera, *Chemical Society Reviews*, 2010, **39**, 4146-4157.
57. W. S. Hummers and R. E. Offeman, *Journal of the American Chemical Society*, 1958, **80**, 1339-1339.
58. D. C. Marcano, D. V. Kosynkin, J. M. Berlin, A. Sinitskii, Z. Z. Sun, A. Slesarev, L. B. Alemany, W. Lu and J. M. Tour, *Acs Nano*, 2010, **4**, 4806-4814.
59. K. Erickson, R. Erni, Z. Lee, N. Alem, W. Gannett and A. Zettl, *Adv. Mater.*, 2010, **22**, 4467-4472.
60. G. Eda and M. Chhowalla, *Adv. Mater.*, 2010, **22**, 2392-2415.
61. K. P. Loh, Q. L. Bao, G. Eda and M. Chhowalla, *Nature Chemistry*, 2010, **2**, 1015-1024.
62. G. Eda, C. Mattevi, H. Yamaguchi, H. Kim and M. Chhowalla, *Journal of Physical Chemistry C*, 2009, **113**, 15768-15771.
63. X. C. Dong, Y. M. Shi, Y. Zhao, D. M. Chen, J. Ye, Y. G. Yao, F. Gao, Z. H. Ni, T. Yu, Z. X. Shen, Y. X. Huang, P. Chen and L. J. Li, *Physical Review Letters*, 2009, **102**, 135501
64. Y. Hernandez, V. Nicolosi, M. Lotya, F. M. Blighe, Z. Y. Sun, S. De, I. T. McGovern, B. Holland, M. Byrne, Y. K. Gun'ko, J. J. Boland, P. Niraj, G. Duesberg, S. Krishnamurthy, R. Goodhue, J. Hutchison, V. Scardaci, A. C. Ferrari and J. N. Coleman, *Nature Nanotechnology*, 2008, **3**, 563-568.
65. G. P. Keeley, A. O'Neill, N. McEvoy, N. Peltekis, J. N. Coleman and G. S. Duesberg, *Journal of Materials Chemistry*, 2010, **20**, 7864-7869.
66. X. C. Dong, C. Y. Su, W. J. Zhang, J. W. Zhao, Q. D. Ling, W. Huang, P. Chen and L. J. Li, *Physical Chemistry Chemical Physics*, 2010, **12**, 2164-2169.
67. D. C. Wei and Y. Q. Liu, *Adv. Mater.*, 2010, **22**, 3225-3241.
68. H. T. Liu, Y. Q. Liu and D. B. Zhu, *Journal of Materials Chemistry*, 2011, **21**, 3335-3345.
69. J. W. Bai and Y. Huang, *Materials Science & Engineering R-Reports*, 2010, **70**, 341-353.
70. L. Y. J. L. Y. Jiao, X. R. Wang, G. Diankov, H. L. Wang and H. J. Dai, *Nature Nanotechnology*, 2010, **5**, 321-325.
71. A. L. Higginbotham, D. V. Kosynkin, A. Sinitskii, Z. Z. Sun and J. M. Tour, *Acs Nano*, 2010, **4**, 2059-2069.
72. A. G. Cano-Marquez, F. J. Rodriguez-Macias, J. Campos-Delgado, C. G. Espinosa-Gonzalez, F. Tristan-Lopez, D. Ramirez-Gonzalez, D. A. Cullen, D. J. Smith, M. Terrones and Y. I. Vega-Cantu, *Nano Letters*, 2009, **9**, 1527-1533.
73. L. C. Campos, V. R. Manfrinato, J. D. Sanchez-Yamagishi, J. Kong and P. Jarillo-Herrero, *Nano Letters*, 2009, **9**, 2600-2604.
74. L. Y. Jiao, L. Zhang, X. R. Wang, G. Diankov and H. J. Dai, *Nature*, 2009, **458**, 877-880.
75. A. V. Talyzin, S. Luzan, I. V. Anoshkin, A. G. Nasibulin, H. Jiang, E. I. Kauppinen, V. M. Mikoushkin, V. V. Shnitov, D. E. Marchenko and D. Noreus, *Acs Nano*, 2011, **5**, 5132-5140.
76. D. B. Shinde, J. Debgupta, A. Kushwaha, M. Aslam and V. K. Pillai, *Journal of the American Chemical Society*, 2011, **133**, 4168-4171.
77. K. Kim, A. Sussman and A. Zettl, *Acs Nano*, 2010, **4**, 1362-1366.
78. P. Kumar, L. S. Panchakarla and C. N. R. Rao, *Nanoscale*, 2011, **3**, 2127-2129.
79. M. Sprinkle, M. Ruan, Y. Hu, J. Hankinson, M. Rubio-Roy, B. Zhang, X. Wu, C. Berger and W. A. de Heer, *Nature Nanotechnology*, 2010, **5**, 727-731.
80. J. M. Cai, P. Ruffieux, R. Jaafar, M. Bieri, T. Braun, S. Blankenburg, M. Muoth, A. P. Seitsonen, M. Saleh, X. L. Feng, K. Mullen and R. Fasel, *Nature*, 2010, **466**, 470-473.
81. Z. H. Chen, Y. M. Lin, M. J. Rooks and P. Avouris, *Physica E-Low-Dimensional Systems & Nanostructures*, 2007, **40**, 228-232.
82. T. Ihn, J. Guttinger, F. Molitor, S. Schnez, E. Schurtenberger, A. Jacobsen, S. Hellmuller, T. Frey, S. Droscher, C. Stampfer and K. Ensslin, *Materials Today*, 2010, **13**, 44-50.
83. L. A. Ponomarenko, F. Schedin, M. I. Katsnelson, R. Yang, E. W. Hill, K. S. Novoselov and A. K. Geim, *Science*, 2008, **320**, 356-358.
84. C. Stampfer, E. Schurtenberger, F. Molitor, J. Guttinger, T. Ihn and K. Ensslin, *Nano Letters*, 2008, **8**, 2378-2383.
85. D. Y. Pan, J. C. Zhang, Z. Li and M. H. Wu, *Adv. Mater.*, 2010, **22**, 734-738.
86. Y. B. Zhang, T. T. Tang, C. Girit, Z. Hao, M. C. Martin, A. Zettl, M. F. Crommie, Y. R. Shen and F. Wang, *Nature*, 2009, **459**, 820-823.
87. X. Huang, Z. Yin, S. Wu, X. Qi, Q. He, Q. Zhang, Q. Yan, F. Boey and H. Zhang, *Small*, 2011, **7**, 1876-1902.
88. W. Choi, I. Lahiri, R. Seelaboyina and Y. S. Kang, *Critical Reviews in Solid State and Materials Sciences*, 2010, **35**, 52-71.
89. D. R. Dreyer, R. S. Ruoff and C. W. Bielawski, *Angewandte Chemie-International Edition*, 2010, **49**, 9336-9344.
90. S. J. Guo and S. J. Dong, *Chemical Society Reviews*, 2011, **40**, 2644-2672.
91. C. N. R. Rao, K. S. Subrahmanyam, H. Matte and A. Govindaraj, *Modern Physics Letters B*, 2011, **25**, 427-451.
92. X. Cui, C. Z. Zhang, R. Hao and Y. L. Hou, *Nanoscale*, 2011, **3**, 2118-2126.
93. M. Terrones, A. R. Botello-Mendez, J. Campos-Delgado, F. Lopez-Urias, Y. I. Vega-Cantu, F. J. Rodriguez-Macias, A. L. Elias, E. Munoz-Sandoval, A. G. Cano-Marquez, J. C. Charlier and H. Terrones, *Nano Today*, 2010, **5**, 351-372.
94. P. Singh, S. Campidelli, S. Giordani, D. Bonifazi, A. Bianco and M. Prato, *Chemical Society Reviews*, 2009, **38**, 2214-2230.
95. B. K. Gorityala, J. M. Ma, X. Wang, P. Chen and X. W. Liu, *Chemical Society Reviews*, 2010, **39**, 2925-2934.
96. Y. Wang, Z. H. Li, J. Wang, J. H. Li and Y. H. Lin, *Trends in Biotechnology*, 2011, **29**, 205-212.
97. W. Yu, H. Xie, L. Chen and Y. Li, Symposium on Photonics and Optoelectronic (SOPO), June 2010, DOI: 10.1109/SOPO.2010.5504403 .

98. Y. L. Zhao and J. F. Stoddart, *Accounts of Chemical Research*, 2009, **42**, 1161-1171.
99. B. G. Choi, H. Park, M. H. Yang, Y. M. Jung, S. Y. Lee, W. H. Hong and T. J. Park, *Nanoscale*, 2010, **2**, 2692-2697.
100. N. Mohanty and V. Berry, *Nano Letters*, 2008, **8**, 4469-4476.
101. S. F. Hou, M. L. Kasner, S. J. Su, K. Patel and R. Cuellari, *Journal of Physical Chemistry C*, 2010, **114**, 14915-14921.
102. J. J. Stephenson, A. K. Sadana, A. L. Higginbotham and J. M. Tour, *Chemistry of Materials*, 2006, **18**, 4658-4661.
103. L. H. Liu, M. M. Lerner and M. D. Yan, *Nano Letters*, 2010, **10**, 3754-3756.
104. C.-Y. Hong, Y.-Z. You and C.-Y. Pan, *Polymer*, 2006, **47**, 4300-4309.
105. Y. Huang, X. Dong, Y. Liu, L.-J. Li and P. Chen, *Journal of Materials Chemistry*, 2011, **21**, 12358-12362.
106. Y. X. Huang, X. C. Dong, Y. M. Shi, C. M. Li, L. J. Li and P. Chen, *Nanoscale*, 2010, **2**, 1485-1488.
107. X. C. Dong, W. Huang and P. Chen, *Nanoscale Research Letters*, 2011, **6**, 60.
108. X. Z. Zhou, X. Huang, X. Y. Qi, S. X. Wu, C. Xue, F. Y. C. Boey, Q. Y. Yan, P. Chen and H. Zhang, *Journal of Physical Chemistry C*, 2009, **113**, 10842-10846.
109. S. Mao, G. H. Lu, K. H. Yu, Z. Bo and J. H. Chen, *Adv. Mater.*, 2010, **22**, 3521-3526.
110. H. Wu, J. Wang, X. H. Kang, C. M. Wang, D. H. Wang, J. Liu, I. A. Aksay and Y. H. Lin, *Talanta*, 2009, **80**, 403-406.
111. Y. Y. Shao, J. Wang, H. Wu, J. Liu, I. A. Aksay and Y. H. Lin, *Electroanalysis*, 2010, **22**, 1027-1036.
112. M. Zhou, Y. Zhai and S. Dong, *Analytical Chemistry*, 2009, **81**, 5603-5613.
113. A. Ambrosi and M. Pumera, *Chemistry – A European Journal*, 2010, **16**, 10946-10949.
114. R. L. McCreery, *Chemical Reviews*, 2008, **108**, 2646-2687.
115. L. Tang, Y. Wang, Y. Li, H. Feng, J. Lu and J. Li, *Advanced Functional Materials*, 2009, **19**, 2782-2789.
116. X. L. Zuo, S. J. He, D. Li, C. Peng, Q. Huang, S. P. Song and C. H. Fan, *Langmuir*, 2010, **26**, 1936-1939.
117. Z. Zhong, W. Wu, D. Wang, D. Wang, J. Shan, Y. Qing and Z. Zhang, *Biosensors and Bioelectronics*, 2010, **25**, 2379-2383.
118. H. F. Xu, H. Dai and G. N. Chen, *Talanta*, 2010, **81**, 334-338.
119. Q. Lu, X. C. Dong, L. J. Li and X. A. Hu, *Talanta*, 2010, **82**, 1344-1348.
120. Q. O. Zeng, J. S. Cheng, L. H. Tang, X. F. Liu, Y. Z. Liu, J. H. Li and J. H. Jiang, *Advanced Functional Materials*, 2010, **20**, 3366-3372.
121. W. Lv, M. Guo, M. H. Liang, F. M. Jin, L. Cui, L. J. Zhi and Q. H. Yang, *Journal of Materials Chemistry*, 2010, **20**, 6668-6673.
122. Q. A. Zhang, Y. Qiao, F. Hao, L. Zhang, S. Y. Wu, Y. Li, J. H. Li and X. M. Song, *Chemistry-a European Journal*, 2010, **16**, 8133-8139.
123. S. J. Guo, D. Wen, Y. M. Zhai, S. J. Dong and E. K. Wang, *Acs Nano*, 2010, **4**, 3959-3968.
124. L. Qian and X. R. Yang, *Talanta*, 2006, **68**, 721-727.
125. M. Zhou, L. Shang, B. L. Li, L. J. Huang and S. J. Dong, *Biosensors & Bioelectronics*, 2008, **24**, 442-447.
126. S. J. Guo, J. Li, W. Ren, D. Wen, S. J. Dong and E. K. Wang, *Chemistry of Materials*, 2009, **21**, 2247-2257.
127. Y. X. Fang, S. J. Guo, C. Z. Zhu, Y. M. Zhai and E. K. Wang, *Langmuir*, 2010, **26**, 11277-11282.
128. Y. Zhou, S. Liu, H. J. Jiang, H. Yang and H. Y. Chen, *Electroanalysis*, 2010, **22**, 1323-1328.
129. L. Y. Cao, Y. L. Liu, B. H. Zhang and L. H. Lu, *Acs Applied Materials & Interfaces*, 2010, **2**, 2339-2346.
130. X. H. Kang, J. Wang, H. Wu, I. A. Aksay, J. Liu and Y. H. Lin, *Biosensors & Bioelectronics*, 2009, **25**, 901-905.
131. C. Cai and J. Chen, *Analytical Biochemistry*, 2004, **332**, 75-83.
132. X. Luo, A. J. Killard and M. R. Smyth, *Electroanalysis*, 2006, **18**, 1131-1134.
133. P. Wu, Q. A. Shao, Y. J. Hu, J. A. Jin, Y. J. Yin, H. Zhang and C. X. Cai, *Electrochim. Acta*, 2010, **55**, 8606-8614.
134. S. Alwarappan, C. Liu, A. Kumar and C. Z. Li, *Journal of Physical Chemistry C*, 2010, **114**, 12920-12924.
135. G. H. Zeng, Y. B. Xing, J. A. Gao, Z. Q. Wang and X. Zhang, *Langmuir*, 2010, **26**, 15022-15026.
136. C. S. Shan, H. F. Yang, J. F. Song, D. X. Han, A. Ivaska and L. Niu, *Analytical Chemistry*, 2009, **81**, 2378-2382.
137. M. H. Yang, B. G. Choi, H. Park, W. H. Hong, S. Y. Lee and T. J. Park, *Electroanalysis*, 2010, **22**, 1223-1228.
138. C. S. Shan, H. F. Yang, D. X. Han, Q. X. Zhang, A. Ivaska and L. Niu, *Biosensors & Bioelectronics*, 2010, **25**, 1070-1074.
139. Y. Y. Shao, S. Zhang, M. H. Engelhard, G. S. Li, G. C. Shao, Y. Wang, J. Liu, I. A. Aksay and Y. H. Lin, *Journal of Materials Chemistry*, 2010, **20**, 7491-7496.
140. Y. Wang, Y. Y. Shao, D. W. Matson, J. H. Li and Y. H. Lin, *Acs Nano*, 2010, **4**, 1790-1798.
141. K. J. Huang, D. J. Niu, J. Y. Sun, C. H. Han, Z. W. Wu, Y. L. Li and X. Q. Xiong, *Colloids and Surfaces B-Biointerfaces*, 2011, **82**, 543-549.
142. H. S. Yin, Y. L. Zhou, Q. A. Ma, S. Y. Ai, Q. P. Chen and L. S. Zhu, *Talanta*, 2010, **82**, 1193-1199.
143. M. Du, T. Yang and K. Jiao, *Journal of Materials Chemistry*, 2010, **20**, 9253-9260.
144. A. Ambrosi and M. Pumera, *Physical Chemistry Chemical Physics*, 2010, **12**, 8944-8948.
145. C. X. Lim, H. Y. Hoh, P. K. Ang and K. P. Loh, *Analytical Chemistry*, 2010, **82**, 7387-7393.
146. M. Muti, S. Sharma, A. Erdem and P. Papakonstantinou, *Electroanalysis*, 2011, **23**, 272-279.
147. J. Zhao, G. F. Chen, L. Zhu and G. X. Li, *Electrochemistry Communications*, 2011, **13**, 31-33.
148. Z. Wang, J. Zhang, P. Chen, X. Zhou, Y. Yang, S. Wu, L. Niu, Y. Han, L. Wang, P. Chen, F. Boey, Q. Zhang, B. Liedberg and H. Zhang, *Biosensors and Bioelectronics*, 2011, **26**, 3881-3886.
149. J. Zhang, J. P. Lei, R. Pan, Y. D. Xue and H. X. Ju, *Biosensors & Bioelectronics*, 2010, **26**, 371-376.
150. B. L. Su, J. A. Tang, J. X. Huang, H. H. Yang, B. Qiu, G. N. Chen and D. P. Tang, *Electroanalysis*, 2010, **22**, 2720-2728.
151. Q. Wei, K. X. Mao, D. Wu, Y. X. Dai, J. A. Yang, B. Du, M. H. Yang and H. Li, *Sensors and Actuators B-Chemical*, 2010, **149**, 314-318.

152.D. Du, Z. X. Zou, Y. S. Shin, J. Wang, H. Wu, M. H. Engelhard, J. Liu, I. A. Aksay and Y. H. Lin, *Analytical Chemistry*, 2010, **82**, 2989-2995.

153.M. H. Yang, A. Javadi, H. Li and S. Q. Gong, *Biosensors & Bioelectronics*, 2010, **26**, 560-565.

154.X. Yu, B. Munge, V. Patel, G. Jensen, A. Bhirde, J. D. Gong, S. N. Kim, J. Gillespie, J. S. Gutkind, F. Papadimitrakopoulos and J. F. Rusling, *Journal of the American Chemical Society*, 2006, **128**, 11199-11205.

155.G. F. Wang, H. Huang, G. Zhang, X. J. Zhang, B. Fang and L. Wang, *Analytical Methods*, 2010, **2**, 1692-1697.

156.Y. Wang, Y. M. Li, L. H. Tang, J. Lu and J. H. Li, *Electrochemistry Communications*, 2009, **11**, 889-892.

157.L. Tan, K. G. Zhou, Y. H. Zhang, H. X. Wang, X. D. Wang, Y. F. Guo and H. L. Zhang, *Electrochemistry Communications*, 2010, **12**, 557-560.

158.W. J. Hong, H. Bai, Y. X. Xu, Z. Y. Yao, Z. Z. Gu and G. Q. Shi, *Journal of Physical Chemistry C*, 2010, **114**, 1822-1826.

159.N. G. Shang, P. Papakonstantinou, M. McMullan, M. Chu, A. Stamboulis, A. Potenza, S. S. Dhesi and H. Marchetto, *Advanced Functional Materials*, 2008, **18**, 3506-3514.

160.J. Zhang, R. H. Xue, W. Y. Ong and P. Chen, *Biophysical Journal*, 2009, **97**, 1371-1380.

161.R. S. Dey and C. R. Raj, *Journal of Physical Chemistry C*, 2010, **114**, 21427-21433.

162.L. Y. Feng, Y. Chen, J. S. Ren and X. G. Qu, *Biomaterials*, 2011, **32**, 2930-2937.

163.X. M. Wu, Y. J. Hu, J. Jin, N. L. Zhou, P. Wu, H. Zhang and C. X. Cai, *Analytical Chemistry*, 2010, **82**, 3588-3596.

164.C. X. Guo, X. T. Zheng, Z. S. Lu, X. W. Lou and C. M. Li, *Adv. Mater.*, 2010, **22**, 5164-5167.

165.B. G. Choi, H. Park, T. J. Park, M. H. Yang, J. S. Kim, S. Y. Jang, N. S. Heo, S. Y. Lee, J. Kong and W. H. Hong, *Acs Nano*, 2010, **4**, 2910-2918.

166.L. Wang, X. H. Zhang, H. Y. Xiong and S. F. Wang, *Biosensors & Bioelectronics*, 2010, **26**, 991-995.

167.J. Li, S. J. Guo, Y. M. Zhai and E. K. Wang, *Analytica Chimica Acta*, 2009, **649**, 196-201.

168.J. Li, S. J. Guo, Y. M. Zhai and E. K. Wang, *Electrochemistry Communications*, 2009, **11**, 1085-1088.

169.J. M. Gong, T. Zhou, D. D. Song and L. Z. Zhang, *Sensors and Actuators B-Chemical*, 2010, **150**, 491-497.

170.H. J. Du, J. S. Ye, J. Q. Zhang, X. D. Huang and C. Z. Yu, *Journal of Electroanalytical Chemistry*, 2011, **650**, 209-213.

171.T. A. Gan, C. G. Hu, Z. L. Chen and S. S. Hu, *Sensors and Actuators B-Chemical*, 2010, **151**, 8-14.

172.C. Wang, L. Zhang, Z. H. Guo, J. G. Xu, H. Y. Wang, K. F. Zhai and X. Zhuo, *Microchimica Acta*, 2010, **169**, 1-6.

173.X. H. Kang, J. Wang, H. Wu, J. Liu, I. A. Aksay and Y. H. Lin, *Talanta*, 2010, **81**, 754-759.

174.H. S. Yin, Q. A. Ma, Y. L. Zhou, S. Y. Ai and L. S. Zhu, *Electrochim. Acta*, 2010, **55**, 7102-7108.

175.J. A. Li, J. H. Chen, X. L. Zhang, C. H. Lu and H. H. Yang, *Talanta*, 2010, **83**, 553-558.

176.H. J. Du, J. S. Ye, J. Q. Zhang, X. D. Huang and C. Z. Yu, *Electroanalysis*, 2010, **22**, 2399-2406.

177.C. S. Shan, H. F. Yang, D. X. Han, Q. X. Zhang, A. Ivaska and L. Niu, *Biosensors & Bioelectronics*, 2010, **25**, 1504-1508.

178.C. X. Guo, Z. S. Lu, Y. Lei and C. M. Li, *Electrochemistry Communications*, 2010, **12**, 1237-1240.

179.T. S. Pui, A. Agarwal, F. Ye, N. Balasubramanian and P. Chen, *Small*, 2009, **5**, 208-212.

180.T. S. Pui, A. Agarwal, F. Ye, Z. Q. Ton, Y. X. Huang and P. Chen, *Nanoscale*, 2009, **1**, 159-163.

181.T. S. Pui, A. Agarwal, F. Ye, Y. X. Huang and P. Chen, *Biosensors & Bioelectronics*, 2011, **26**, 2746-2750.

182.V. Barone, O. Hod and G. E. Scuseria, *Nano Letters*, 2006, **6**, 2748-2754.

183.M. Han, B. Ozyilmaz, Y. Zhang, P. Jarillo-Herero and P. Kim, *Physica Status Solidi B-Basic Solid State Physics*, 2007, **244**, 4134-4137.

184.X. C. Dong, D. L. Fu, W. J. Fang, Y. M. Shi, P. Chen and L. J. Li, *Small*, 2009, **5**, 1422-1426.

185.D. C. Wei, Y. Q. Liu, Y. Wang, H. L. Zhang, L. P. Huang and G. Yu, *Nano Letters*, 2009, **9**, 1752-1758.

186.S. Agarwal, X. Z. Zhou, F. Ye, Q. Y. He, G. C. K. Chen, J. Soo, F. Boey, H. Zhang and P. Chen, *Langmuir*, 2010, **26**, 2244-2247.

187.M. Kalbacova, A. Broz, J. Kong and M. Kalbac, *Carbon*, 2010, **48**, 4323-4329.

188.A. Das, S. Pisana, B. Chakraborty, S. Piscanec, S. K. Saha, U. V. Waghmare, K. S. Novoselov, H. R. Krishnamurthy, A. K. Geim, A. C. Ferrari and A. K. Sood, *Nature Nanotechnology*, 2008, **3**, 210-215.

189.F. Chen, Q. Qing, J. L. Xia and N. J. Tao, *Chemistry-an Asian Journal*, 2010, **5**, 2144-2153.

190.T. O. Wehling, K. S. Novoselov, S. V. Morozov, E. E. Vdovin, M. I. Katsnelson, A. K. Geim and A. I. Lichtenstein, *Nano Letters*, 2008, **8**, 173-177.

191.H. Pinto, R. Jones, J. P. Goss and P. R. Briddon, *physica status solidi (a)*, 2010, **207**, 2131-2136.

192.M. Myers, J. Cooper, B. Pejcic, M. Baker, B. Raguse and L. Wieczorek, *Sensors and Actuators B-Chemical*, 2011, **155**, 154-158.

193.S. Adam, E. H. Hwang, V. M. Galitski and S. Das Sarma, *Proceedings of the National Academy of Sciences of the United States of America*, 2007, **104**, 18392-18397.

194.F. Chen, J. L. Xia, D. K. Ferry and N. J. Tao, *Nano Letters*, 2009, **9**, 2571-2574.

195.S. K. Saha, R. C. Chandrakanth, H. R. Krishnamurthy and U. V. Waghmare, *Physical Review B*, 2009, **80**, 155414

196.W. Z. Bao, F. Miao, Z. Chen, H. Zhang, W. Y. Jang, C. Dames and C. N. Lau, *Nature Nanotechnology*, 2009, **4**, 562-566.

197.A. L. V. de Parga, F. Calleja, B. Borca, M. C. G. Passeggi, J. J. Hinarejos, F. Guinea and R. Miranda, *Physical Review Letters*, 2008, **100**, 056807

198.G. H. Lu, L. E. Ocola and J. H. Chen, *Nanotechnology*, 2009, **20**, 445502

199.H. Y. Jeong, D. S. Lee, H. K. Choi, D. H. Lee, J. E. Kim, J. Y. Lee, W. J. Lee, S. O. Kim and S. Y. Choi, *Applied Physics Letters*, 2010, **96**, 3432446

200.G. H. Lu, L. E. Ocola and J. H. Chen, *Applied Physics Letters*, 2009, **94**, 3086896

201.V. Dua, S. P. Surwade, S. Ammu, S. R. Agnihotra, S. Jain, K. E. Roberts, S. Park, R. S. Ruoff and S. K. Manohar, *Angewandte Chemie-International Edition*, 2010, **49**, 2154-2157.

202.J. D. Fowler, M. J. Allen, V. C. Tung, Y. Yang, R. B. Kaner and B. H. Weiller, *Acs Nano*, 2009, **3**, 301-306.

203.M. W. K. Nomani, R. Shishir, M. Qazi, D. Diwan, V. B. Shields, M. G. Spencer, G. S. Tompa, N. M. Sbrockey and G. Koley, *Sensors and Actuators B-Chemical*, 2010, **150**, 301-307.

204.G. Ko, H. Y. Kim, J. Ahn, Y. M. Park, K. Y. Lee and J. Kim, *Current Applied Physics*, 2010, **10**, 1002-1004.

205.J. T. Robinson, F. K. Perkins, E. S. Snow, Z. Q. Wei and P. E. Sheehan, *Nano Letters*, 2008, **8**, 3137-3140.

206.M. Shafiei, P. G. Spizzirri, R. Arsat, J. Yu, J. du Plessis, S. Dubin, R. B. Kaner, K. Kalantar-Zadeh and W. Wlodarski, *Journal of Physical Chemistry C*, 2010, **114**, 13796-13801.

207.L. S. Zhang, W. D. Wang, X. Q. Liang, W. S. Chu, W. G. Song, W. Wang and Z. Y. Wu, *Nanoscale*, 2011, **3**, 2458-2460.

208.J. L. Johnson, A. Behnam, S. J. Pearton and A. Ural, *Adv. Mater.*, 2010, **22**, 4877-4880.

209.E. Massera, V. La Ferrara, M. Miglietta, T. Polichetti, I. Nasti and G. Di Francia, *Chimica Oggi-Chemistry Today*, 2011, **29**, 39-41.

210.J. L. Zhang, G. X. Shen, W. J. Wang, X. J. Zhou and S. W. Guo, *Journal of Materials Chemistry*, 2010, **20**, 10824-10828.

211.T. V. Cuong, V. H. Pham, J. S. Chung, E. W. Shin, D. H. Yoo, S. H. Hahn, J. S. Huh, G. H. Rue, E. J. Kim, S. H. Hur and P. A. Kohl, *Materials Letters*, 2010, **64**, 2479-2482.

212.G. Lu, K. Yu, L. E. Ocola and J. Chen, *Chemical Communications*, 2011, **47**, 7761-7763.

213.K. H. Yu, P. X. Wang, G. H. Lu, K. H. Chen, Z. Bo and J. H. Chen, *Journal of Physical Chemistry Letters*, 2011, **2**, 537-542.

214.Y. P. Dan, Y. Lu, N. J. Kybert, Z. T. Luo and A. T. C. Johnson, *Nano Letters*, 2009, **9**, 1472-1475.

215.B. H. Chu, J. Nicolosi, C. F. Lo, W. Strupinski, S. J. Pearton and F. Ren, *Electrochemical and Solid-State Letters*, 2011, **14**, K43-K45.

216.J. Yi, J. M. Lee and W. Il Park, *Sensors and Actuators B-Chemical*, 2011, **155**, 264-269.

217.Y. Lu, B. R. Goldsmith, N. J. Kybert and A. T. C. Johnson, *Applied Physics Letters*, 2010, **97**, 3483128

218.P. K. Ang, W. Chen, A. T. S. Wee and K. P. Loh, *Journal of the American Chemical Society*, 2008, **130**, 14392-14393.

219.Y. Ohno, K. Maehashi and K. Matsumoto, *Biosensors & Bioelectronics*, 2010, **26**, 1727-1730.

220.T. Zhang, Z. G. Cheng, Y. B. Wang, Z. J. Li, C. X. Wang, Y. B. Li and Y. Fang, *Nano Letters*, 2010, **10**, 4738-4741.

221.H. G. Sudibya, Q. Y. He, H. Zhang and P. Chen, *Acs Nano*, 2011, **5**, 1990-1994.

222.Y. Ohno, K. Maehashi, Y. Yamashiro and K. Matsumoto, *Nano Letters*, 2009, **9**, 3318-3322.

223.Y. Ohno, K. Maehashi and K. Matsumoto, *Journal of the American Chemical Society*, 2010, **132**, 18012-18013.

224.M. H. Yang and S. Q. Gong, *Chemical Communications*, 2010, **46**, 5796-5798.

225.X. C. Dong, Y. M. Shi, W. Huang, P. Chen and L. J. Li, *Adv. Mater.*, 2010, **22**, 1649-1653.

226.Y. Ohno, K. Maehashi, K. Inoue and K. Matsumoto, *Japanese Journal of Applied Physics*, 2011, **50**, 070120

227.S. Myung, A. Solanki, C. Kim, J. Park, K. S. Kim and K. B. Lee, *Adv. Mater.*, 2011, **23**, 2221-2225.

228.R. Stine, J. T. Robinson, P. E. Sheehan and C. R. Tamanaha, *Adv. Mater.*, 2010, **22**, 5297-5300.

229.T. S. Pui, H. G. Sudibya, X. N. Luan, Q. Zhang, F. Ye, Y. X. Huang and P. Chen, *Adv. Mater.*, 2010, **22**, 3199-3203.

230.N. Shao, E. Wickstrom and B. Panchapakesan, *Nanotechnology*, 2008, **19**, 465101

231.H. G. Sudibya, J. M. Ma, X. C. Dong, S. Ng, L. J. Li, X. W. Liu and P. Chen, *Angewandte Chemie-International Edition*, 2009, **48**, 2723-2726.

232.J. Zhang, D. L. Fu, M. B. Chan-Park, L. J. Li and P. Chen, *Adv. Mater.*, 2009, **21**, 790-793.

233.Q. Qing, S. K. Pal, B. Z. Tian, X. J. Duan, B. P. Timko, T. Cohen-Karni, V. N. Murthy and C. M. Lieber, *Proceedings of the National Academy of Sciences of the United States of America*, 2010, **107**, 1882-1887.

234.F. Patolsky, B. P. Timko, G. H. Yu, Y. Fang, A. B. Greytak, G. F. Zheng and C. M. Lieber, *Science*, 2006, **313**, 1100-1104.

235.T. Cohen-Karni, Q. Qing, Q. Li, Y. Fang and C. M. Lieber, *Nano Letters*, 2010, **10**, 1098-1102.

236.Q. Y. He, H. G. Sudibya, Z. Y. Yin, S. X. Wu, H. Li, F. Boey, W. Huang, P. Chen and H. Zhang, *Acs Nano*, 2010, **4**, 3201-3208.

237.P. Chen and K. D. Gillis, *Biophysical Journal*, 2000, **79**, 2162-2170.

238.P. Chen, T. C. Hwang and K. D. Gillis, *Journal of General Physiology*, 2001, **118**, 135-144.

239.Y. X. Huang, H. G. Sudibya and P. Chen, *Biosensors & Bioelectronics*, 2011, **26**, 4257-4261.

240.R. Kempaiah, A. Chung and V. Maheshwari, *Acs Nano*, 2011, **5**, 6025-6031.

241.X. Zhou, J. M. Moran-Mirabal, H. G. Craighead and P. L. McEuen, *Nat Nano*, 2007, **2**, 185-190.

242.Y. X. Huang, P. V. Palkar, L. J. Li, H. Zhang and P. Chen, *Biosensors & Bioelectronics*, 2010, **25**, 1834-1837.

243.P. K. Ang, M. Jaiswal, C. Lim, Y. Wang, J. Sankaran, A. Li, C. T. Lim, T. Wohland, O. Barbaros and K. P. Loh, *Acs Nano*, 2010, **4**, 7387-7394.

244.Z. G. Cheng, Q. Li, Z. J. Li, Q. Y. Zhou and Y. Fang, *Nano Letters*, 2010, **10**, 1864-1868.

245.M. Dankerl, M. V. Hauf, A. Lippert, L. H. Hess, S. Birner, I. D. Sharp, A. Mahmood, P. Mallet, J. Y. Veuillen, M. Stutzmann and J. A. Garrido, *Advanced Functional Materials*, 2010, **20**, 3117-3124.

246.J. N. Tey, I. P. M. Wijaya, J. Wei, I. Rodriguez and S. G. Mhaisalkar, *Microfluidics and Nanofluidics*, 2010, **9**, 1185-1214.

247.S. K. Min, W. Y. Kim, Y. Cho and K. S. Kim, *Nature Nanotechnology*, 2011, **6**, 162-165.

248.X. Dong, Q. Long, J. Wang, M. B. Chan-Park, Y. Huang, W. Huang and P. Chen, *Nanoscale*, 2011. DOI: 10.1039/c1nr11006c

249.Y. X. Huang, H. G. Sudibya, D. L. Fu, R. H. Xue, X. C. Dong, L. J. Li and P. Chen, *Biosensors & Bioelectronics*, 2009, **24**, 2716-2720.

250.L. X. Chen, S. F. Xu and J. H. Li, *Chemical Society Reviews*, 2011, **40**, 2922-2942.

251.D. Cai, L. Ren, H. Z. Zhao, C. J. Xu, L. Zhang, Y. Yu, H. Z. Wang, Y. C. Lan, M. F. Roberts, J. H. Chuang, M. J. Naughton, Z. F. Ren and T. C. Chiles, *Nature Nanotechnology*, 2010, **5**, 597-601.

252.Z. T. Luo, P. M. Vora, E. J. Mele, A. T. C. Johnson and J. M. Kikkawa, *Applied Physics Letters*, 2009, **94**, 111909

253.X. M. Sun, Z. Liu, K. Welsher, J. T. Robinson, A. Goodwin, S. Zaric and H. J. Dai, *Nano Research*, 2008, **1**, 203-212.

254.Z. F. Liu, Q. Liu, Y. Huang, Y. F. Ma, S. G. Yin, X. Y. Zhang, W. Sun and Y. S. Chen, *Adv. Mater.*, 2008, **20**, 3924-3930.

255.J. Kim, L. J. Cote, F. Kim and J. X. Huang, *Journal of the American Chemical Society*, 2010, **132**, 260-267.

256.J. L. Chen and X. P. Yan, *Journal of Materials Chemistry*, 2010, **20**, 4328-4332.

257.K. S. Subrahmanyam, P. Kumar, A. Nag and C. N. R. Rao, *Solid State Communications*, 2010, **150**, 1774-1777.

258.L. M. Xie, X. Ling, Y. Fang, J. Zhang and Z. F. Liu, *Journal of the American Chemical Society*, 2009, **131**, 9890-9891.

259.X. L. X. Ling, L. M. Xie, Y. Fang, H. Xu, H. L. Zhang, J. Kong, M. S. Dresselhaus, J. Zhang and Z. F. Liu, *Nano Letters*, 2010, **10**, 553-561.

260.Z. W. Tang, H. Wu, J. R. Cort, G. W. Buchko, Y. Y. Zhang, Y. Y. Shao, I. A. Aksay, J. Liu and Y. H. Lin, *Small*, 2010, **6**, 1205-1209.

261.C. H. Lu, J. Li, J. J. Liu, H. H. Yang, X. Chen and G. N. Chen, *Chemistry-a European Journal*, 2010, **16**, 4889-4894.

262.J. W. Yi, J. Park, N. J. Singh, I. J. Lee, K. S. Kim and B. H. Kim, *Bioorganic & Medicinal Chemistry Letters*, 2011, **21**, 704-706.

263.F. Li, Y. Huang, Q. Yang, Z. T. Zhong, D. Li, L. H. Wang, S. P. Song and C. H. Fan, *Nanoscale*, 2010, **2**, 1021-1026.

264.H. F. Dong, W. C. Gao, F. Yan, H. X. Ji and H. X. Ju, *Analytical Chemistry*, 2010, **82**, 5511-5517.

265.S. Jiang, A. Liu, H. Duan, J. Soo and P. Chen, *Advanced Functional Materials*, 2011, **21**, 2776-2780.

266.C. H. Lu, H. H. Yang, C. L. Zhu, X. Chen and G. N. Chen, *Angewandte Chemie-International Edition*, 2009, **48**, 4785-4787.

267.S. D. Jhaveri, R. Kirby, R. Conrad, E. J. Maglott, M. Bowser, R. T. Kennedy, G. Glick and A. D. Ellington, *Journal of the American Chemical Society*, 2000, **122**, 2469-2473.

268.R. H. Yang, Z. W. Tang, J. L. Yan, H. Z. Kang, Y. M. Kim, Z. Zhu and W. H. Tan, *Analytical Chemistry*, 2008, **80**, 7408-7413.

269.H. X. Chang, L. H. Tang, Y. Wang, J. H. Jiang and J. H. Li, *Analytical Chemistry*, 2010, **82**, 2341-2346.

270.X. H. Wang, C. Y. Wang, K. G. Qu, Y. J. Song, J. S. Ren, D. Miyoshi, N. Sugimoto and X. G. Qu, *Advanced Functional Materials*, 2010, **20**, 3967-3971.

271.Y. Wang, Z. H. Li, D. H. Hu, C. T. Lin, J. H. Li and Y. H. Lin, *Journal of the American Chemical Society*, 2010, **132**, 9274-9276.

272.Y. Q. Wen, F. F. Xing, S. J. He, S. P. Song, L. H. Wang, Y. T. Long, D. Li and C. H. Fan, *Chemical Communications*, 2010, **46**, 2596-2598.

273.S. J. He, B. Song, D. Li, C. F. Zhu, W. P. Qi, Y. Q. Wen, L. H. Wang, S. P. Song, H. P. Fang and C. H. Fan, *Advanced Functional Materials*, 2010, **20**, 453-459.

274.B. Dubertret, M. Calame and A. J. Libchaber, *Nature Biotechnology*, 2001, **19**, 365-370.

275.S. Tyagi and F. R. Kramer, *Nature Biotechnology*, 1996, **14**, 303-308.

276.H. X. Li and L. Rothberg, *Proceedings of the National Academy of Sciences of the United States of America*, 2004, **101**, 14036-14039.

277.R. H. Yang, J. Y. Jin, Y. Chen, N. Shao, H. Z. Kang, Z. Xiao, Z. W. Tang, Y. R. Wu, Z. Zhu and W. H. Tan, *Journal of the American Chemical Society*, 2008, **130**, 8351-8358.

278.J. Balapanuru, J. X. Yang, S. Xiao, Q. L. Bao, M. Jahan, L. Polavarapu, J. Wei, Q. H. Xu and K. P. Loh, *Angewandte Chemie-International Edition*, 2010, **49**, 6549-6553.

279.L. P. Cai, R. Y. Zhan, K. Y. Pu, X. Y. Qi, H. Zhang, W. Huang and B. Liu, *Analytical Chemistry*, 2011, **83**, 7849-7855.

280.C. L. Zhang, Y. X. Yuan, S. M. Zhang, Y. H. Wang and Z. H. Liu, *Angewandte Chemie-International Edition*, 2011, **50**, 6851-6854.

281.X. H. Zhao, R. M. Kong, X. B. Zhang, H. M. Meng, W. N. Liu, W. H. Tan, G. L. Shen and R. Q. Yu, *Analytical Chemistry*, 2011, **83**, 5062-5066.

282.Y. Q. Wen, C. Peng, D. Li, L. Zhuo, S. J. He, L. H. Wang, Q. Huang, Q. H. Xu and C. H. Fan, *Chemical Communications*, 2011, **47**, 6278-6280.

283.F. Liu, J. Y. Choi and T. S. Seo, *Biosensors & Bioelectronics*, 2010, **25**, 2361-2365.

284.J. H. Jung, D. S. Cheon, F. Liu, K. B. Lee and T. S. Seo, *Angewandte Chemie-International Edition*, 2010, **49**, 5708-5711.

285.L. Wu, H. S. Chu, W. S. Koh and E. P. Li, *Optics Express*, 2010, **18**, 14395-14400.

286.S. H. Choi, Y. L. Kim and K. M. Byun, *Optics Express*, 2011, **19**, 458-466.

287.L. Wang, C. Z. Zhu, L. Han, L. H. Jin, M. Zhou and S. J. Dong, *Chemical Communications*, 2011, **47**, 7794-7796.

288.Y. X. Xu, L. Zhao, H. Bai, W. J. Hong, C. Li and G. Q. Shi, *Journal of the American Chemical Society*, 2009, **131**, 13490-13497.

289.Y. J. Song, K. G. Qu, C. Zhao, J. S. Ren and X. G. Qu, *Adv. Mater.*, 2010, **22**, 2206-2210.

290.Y. Wang, J. Lu, L. Tang, H. Chang and J. Li, *Analytical Chemistry*, 2009, **81**, 9710-9715.

291.S. Xu, Y. Liu, T. Wang and J. Li, *Analytical Chemistry*, 2011, **83**, 3817-3823.

292.G. Lu, H. Li, C. Liusman, Z. Yin, S. Wu and H. Zhang, *Chemical Science*, 2011, **2**, 1817-1821.

293.W. Ren, Y. X. Fang and E. K. Wang, *Acs Nano*, 2011, **5**, 6425-6433.

294.P. Chen and C. M. Li, *Small*, 2007, **3**, 1204-1208.

295.A. Meller, L. Nivon, E. Brandin, J. Golovchenko and D. Branton, *Proceedings of the National Academy of Sciences of the United States of America*, 2000, **97**, 1079-1084.

296.P. Chen, T. Mitsui, D. B. Farmer, J. Golovchenko, R. G. Gordon and D. Branton, *Nano Letters*, 2004, **4**, 1333-1337.

297.Y. R. Kim, C. M. Li, Q. Wang and P. Chen, *Frontiers in Bioscience*, 2007, **12**, 2978-2983.

298.C. A. Merchant, K. Healy, M. Wanunu, V. Ray, N. Peterman, J. Bartel, M. D. Fischbein, K. Venta, Z. T. Luo, A. T. C. Johnson and M. Drndic, *Nano Letters*, 2010, **10**, 2915-2921.

299.G. F. Schneider, S. W. Kowalczyk, V. E. Calado, G. Pandraud, H. W. Zandbergen, L. M. K. Vandersypen and C. Dekker, *Nano Letters*, 2010, **10**, 3163-3167.

300.S. Garaj, W. Hubbard, A. Reina, J. Kong, D. Branton and J. A. Golovchenko, *Nature*, 2010, **467**, 190-193.

301.D. Branton, D. W. Deamer, A. Marziali, H. Bayley, S. A. Benner, T. Butler, M. Di Ventra, S. Garaj, A. Hibbs, X. H. Huang, S. B. Jovanovich, P. S. Krstic, S. Lindsay, X. S. S. Ling, C. H. Mastrangelo, A. Meller, J. S. Oliver, Y. V. Pershin, J. M. Ramsey, R. Riehn, G. V. Soni, V. Tabard-Cossa, M. Wanunu, M. Wiggin and J. A. Schloss, *Nature Biotechnology*, 2008, **26**, 1146-1153.

302.T. Nelson, B. Zhang and O. V. Prezhdo, *Nano Letters*, 2010, **10**, 3237-3242.

303.F. P. Ouyang, S. L. Peng, H. Zhang, L. B. Weng and H. Xu, *Chinese Physics B*, 2011, **20**, 058504

304.H. W. C. Postma, *Nano Letters*, 2010, **10**, 420-425.

305.Y. He, R. H. Scheicher, A. Grigoriev, R. Ahuja, S. Long, Z. Huo and M. Liu, *Advanced Functional Materials*, 2011, **21**, 2674-2679.

306.D. E. Jiang, V. R. Cooper and S. Dai, *Nano Letters*, 2009, **9**, 4019-4024.

307.K. Sint, B. Wang and P. Kral, *Journal of the American Chemical Society*, 2008, **130**, 16448-16449.

308.J. O. Sofo, A. S. Chaudhari and G. D. Barber, *Physical Review B*, 2007, **75**, 153401

309.Z. P. Chen, W. C. Ren, L. B. Gao, B. L. Liu, S. F. Pei and H. M. Cheng, *Nature Materials*, 2011, **10**, 424-428.

310.X. Huang, X. Qi, F. Boey and H. Zhang, *Chemical Society Reviews*, 2012. DOI: 10.1039/C1CS15078B

311.X. Dong, G. Xing, M. B. Chan-Park, W. Shi, N. Xiao, J. Wang, Q. Yan, T. C. Sum, W. Huang and P. Chen, *Carbon*, 2011, **49**, 5071-5078.

312.X. C. Dong, B. Li, A. Wei, X. H. Cao, M. B. Chan-Park, H. Zhang, L. J. Li, W. Huang and P. Chen, *Carbon*, 2011, **49**, 2944-2949.